

**NANYANG
TECHNOLOGICAL
UNIVERSITY**

SINGAPORE

**Development of a platform for low
intensity light detection used for
optical analysis of water purity**

Sun Biniao

SCHOOL OF ELECTRICAL AND ELECTRONIC ENGINEERING

2024

Development of a platform for low intensity light detection used for optical analysis of water purity

SUN BINHAO

SCHOOL OF ELECTRICAL AND ELECTRONIC ENGINEERING

**A DISSERTATION SUBMITTED IN PARTIAL FULFILMENT OF
THE REQUIREMENTS FOR THE DEGREE OF
MASTER OF SCIENCE IN SIGNAL PROCESSING**

2024

Statement of Originality

I hereby certify that the work embodied in this thesis is the result of original research and has not been submitted for a higher degree to any other University or Institution.

.....
14/07/2024
.....

Date

NTU NTU NTU NTU NTU NTU NTU
NTU NTU NTU NTU NTU NTU NTU
NTU NTU NTU NTU NTU NTU NTU
Sun Binhas
NTU NTU NTU NTU NTU NTU NTU
NTU NTU NTU NTU NTU NTU NTU

Your Name

Supervisor Declaration Statement

I have reviewed the content and presentation style of this thesis and declare it is free of plagiarism and of sufficient grammatical clarity to be examined. To the best of my knowledge, the research and writing are those of the candidate except as acknowledged in the Author Attribution Statement. I confirm that the investigations were conducted in accord with the ethics policies and integrity standards of Nanyang Technological University and that the research data are presented honestly and without prejudice

16 July 2024

.....
Date

Poenar Daniel Puiu
A/P Poenar Daniel Puiu
Supervisor's Name

Authorship Attribution Statement

This thesis does not contain any materials from papers published in peer-reviewed journals or from papers accepted at conferences in which I am listed as an author.

14/07/2024

.....
Date

.....
Sun BinHao
.....
Your Name

Table of Contents

Abstract	iii
Acknowledgement	v
Lists of Figures	vii
1 Introduction	1
1.1 Background	1
1.2 Motivation and Objective	2
1.3 Thesis Organization	5
2 Literature Review	8
2.1 Fluorescence	8
2.1.1 Fundamental operation principle	8
2.1.2 Fluorescence detection principle	10
2.1.3 The principle of fluorescence concentration measurement based on the method of light transmission	12
2.1.4 Traditional fluorescence detection	14
2.1.5 Optical spatial filter	16
2.2 Examples of reported fluorescence detection systems	17
2.2.1 LED-Based Fluorescence Detection System	17
2.2.2 Laser-Induced Fluorescence Detection System (LIF)	19
2.2.3 Time-Resolved Fluorescence Immunoassay (TRFIA)	20
2.2.4 Conclusion	22
2.3 Weak signal detection methods	22
2.3.1 Background	22
2.3.2 Correlation Detection	24
2.3.3 Lock-in amplifier	28
2.3.4 Sampling Integration	31
2.3.5 Noise filtering	32
2.3.6 Adaptive Noise Cancellation	32
2.3.7 Photon Counting	32
2.3.8 Instrumentation Amplifier	33
3 Optical System	34
3.1 Optical System Simulation	34
3.1.1 Integrating Sphere Simulated model	34

3.1.2	Mathematical Derivation	35
3.1.3	Zemax Simulation	37
3.1.4	Results	38
3.1.5	Elliptical cylinder optical model	41
3.1.6	Compare two models	43
4	Circuit design	48
4.1	Hardware Circuit Overall Design	48
4.2	Hardware Design	49
4.2.1	Design of the Photoelectric Conversion Circuit	49
4.3	Design of the Preamplifier Circuit	57
4.3.1	General Amplification Circuit	58
4.3.2	T Network Amplification Circuit	58
4.3.3	Instrumentation Amplifiers	61
4.3.4	Design of the Control Unit Circuit	65
4.4	Summary of this Chapter	68
5	Conclusion and Future Work	69
5.1	Conclusion	69
5.2	Future work	70
	References	71

Abstract

As is well-known, Singapore is currently making great efforts for building a robust, diversified and sustainable water supply. Desalination is one of the main methods to obtain drinkable water, but the process lacks on-line procedures/tools to assess water purity easily and rapidly.

This project, in collaboration with NEWRI, explores the tremendous potential to utilize optical analysis (e.g. UV absorbance and/or fluorescence) to monitor the output of the desalination processes and assess the quality of purified water. However, the setup and signal processing circuits used for this purpose need to detect very low light levels. Hence, other methods need to be applied here, very different from the well-known simple transimpedance amplifier for a photodiode, which is feasible only for normal applications when the light intensity is high enough. For instance, lock-in amplifier, or quadrature modulation and detection, or (sometimes even) time-domain photon counting, are among the main types of circuits and methods for signal processing used for such applications.

The dissertation will investigate a few of these methods for processing the signal output from low intensity light detection, assess their advantages and disadvantages, as well as their performance characteristics. In this paper, we will investigate several of these methods for processing the output of low-intensity light detection signals, including which include phase-locked amplification, sampling integration, correlation detection, adaptive noise cancellation, and amplification by differential amplification circuits. Their advantages and disadvantages

as well as their performance characteristics are evaluated. In this paper, a new elliptical low-intensity light detection platform is simulated in Zemax by means of mathematical geometry and design of amplification circuits to detect small differences between the reference light source and the actual light source.

Keywords: low-light detection techniques, ZEMAX, fluorescence, Differential amplifier circuit, lock-in amplifier circuit

Acknowledgements

I would like to extend my heartfelt gratitude to Associate Professor Poenar Daniel Puiu for his invaluable academic guidance and support throughout my research journey. His insights and suggestions have been crucial in shaping my work. I am equally grateful to Mr. Chittoor Sendhilkumar Raghavendhran and Mr. Ronald Wee Jia Yang for their expertise and enthusiastic assistance, which have been indispensable to my research. Additionally, my sincere thanks go to Zhang Run Fan for his warm help and ongoing support. I am also deeply appreciative of the technical support and software access provided by the CAE Laboratory, which were essential for my research. Last but not least, I owe a profound debt of gratitude to my parents for their unwavering support and encouragement. Their belief in me has been the cornerstone of my academic pursuit. They have been my steadfast support at every step of this academic journey.

List of Figures

1.1	Generic fluorescence measurement setup (adapted from [12])	7
2.1	Jablonski diagram illustrating the process involved in the creation of an excited electronic singlet state in fluorescence molecules by optical absorption and subsequent fluorescent light Em(adapted from [19])	9
2.2	Schematic diagram of light beam passing through fluorescence area	12
2.3	Traditional fluorescence microscopy configuration for high sensitivity detection(adapted from [21])	15
2.4	Schematic diagram of LED-induced fluorescence detection system: (1) LED; (2) iris; (3) lens (focal length 6 cm); (4), interference filter (BP 470 nm); (5) dichroic mirror; (6) objective; (7) capillary flow cell; (8) interfere filter (BP 530 nm); (9) lens (focal length 6 cm); (10) photomultiplier tube (PMT); (11) personal computer(adapted from [22])	18
2.5	Schematic diagram of the optical setup of the LED-FD system(adapted from [23])	19
2.6	The optical module of TRFIA system(adapted from [24])	21
2.7	Block diagram of the autocorrelation detection method[33]	25
2.8	Block diagram of the cross-correlation detection method[33]	27
2.9	Block diagram of a lock-in amplifier	29
2.10	Block diagram of a sampling integration process[35]	31
3.1	Integrating sphere optical modeling	35
3.2	Surface coating setting in Zemax as aluminum material	37
3.3	Fluorescent sample	38
3.4	Output detector	39
3.5	Fluorescent material model	39
3.6	The emssion spectrum(Excitation wavvelength:0.4770 microns) . .	40
3.7	The absorption spectrum(peak wavvelength:0.421 microns)	40
3.8	Elliptical cylinder cavity	41
3.9	Elliptical cylinder cavity	42
3.10	Elliptical cylinder optical model	43
3.11	Fluorescence converges at the focal point	44
3.12	Elliptical cylinder model	45
3.13	Integrating sphere model	45

4.1	System Overall Scheme Diagram	48
4.2	PIN photodiode structure	51
4.3	Spectral response curves of photodiodes of common materials	52
4.4	General Optical Detection Circuit	54
4.5	Improved transimpedance amplifier	56
4.6	Transimpedance amplifier	59
4.7	T Network Amplification Circuit	60
4.8	Differential Amplifier Circuit	61
4.9	Instrumentation amplifier[39]	63
4.10	Microcontroller structure block diagram	66
4.11	Microcontroller circuit	67

Chapter 1

Introduction

This passage discusses how fluorescence has been used in water science research over the last 50 years, focusing particularly on studying organic matter in different aquatic environments. Organic matter can be found in various forms like dissolved, colloidal, and particulate states. As is well-known, Singapore is currently making great efforts for building a robust, diversified and sustainable water supply [1]. So, we want to develop a platform for low intensity light detection used for optical analysis of water purity [2].

1.1 Background

When a chemical substance is irradiated by incident light of a specific wavelength, it can store energy and enter an excited state, and at the same time excite another wavelength of emitted light, which is called fluorescence [3]. The generation of fluorescence is predicated on incident light irradiation, and once irradiation is stopped, the fluorescence disappears [4].

Fluorescence analysis is the quantitative or qualitative analysis of the intensity or spectrum of this fluorescence signal. It is an important part of spectroscopy, and its application is increasingly widespread. Compared to other

analytical methods in the field of spectroscopy, the greatest advantage of fluorescence analysis is reflected in its high analytical sensitivity and selectivity for trace substances. Different analytical methods can be used for the qualitative or quantitative analysis of fluorescence signals to measure the properties of the substance to be measured, of which the simplest method is direct determination. The simplest method is direct measurement. As long as the substance itself is able to excite fluorescence, it can be directly analyzed by direct measurement to analyze the properties, concentration and other information of the substance. For other substances that do not emit fluorescent signals, they can only be analyzed by indirect measurement [5].

1.2 Motivation and Objective

Water quality detection technology based on optical methods has the advantages of high sensitivity, fast detection speed, real-time online monitoring, distributed and quasi-distributed monitoring, etc., which is widely used in the field of water quality detection and sensing; at the same time, the water quality detection technology using optical methods is also capable of realizing multi-parameter non-destructive and non-polluting detection, facilitating miniaturization and intelligence, and capable of realizing rapid on-site detection, which is a very promising detection method. Adsorption spectrophotometry is such a very promising optical detection method [6].

However, spectrophotometry has the following disadvantages:

- Selectivity: Keep in mind that a UV/Vis spectrophotometer does not discriminate between the sample of interest and contaminants that absorb at the same wavelength. For example, all nucleic acids exhibit a peak at or around 260 nm; therefore, intact RNA and double-stranded DNA, as well as the degraded species of single-stranded DNA in a sample solution, contribute to total absorbance at 260 nm [7].

- Stray light: The detectors used in spectrophotometers are broadband, meaning they respond to all the light that reaches them. If there are impurities in the sample that reflect light, an erroneous reading may be recorded. Stray light also causes a decrease in absorbance and reduces the linearity range of the instrument [8].
- Sample conditions: Absorption results can be influenced by temperature, pH, impurities, and contaminants. All of these factors can change the absorption properties of the sample, leading to inaccurate readings.
- Low sensitivity: The sensitivity of a spectrophotometer is often inadequate at low sample concentrations. Researchers may need to concentrate their sample, adding additional steps and time to their workflow.

In contrast, optical investigation using fluorescence has the following advantages::

- High Sensitivity: Fluorescence analysis methods have extremely high sensitivity and can detect very low concentrations of samples. Since the intensity of the fluorescence signal is proportional to the intensity of the Ex light, even trace amounts of fluorescent substances can produce detectable signals [9].
- High Selectivity: Fluorescence analysis can distinguish different fluorescent substances by selecting specific Ex and Em wavelengths, thereby achieving high selectivity detection. This allows fluorescence methods to identify specific target substances in complex samples.
- Real-time Detection: Fluorescence analysis can perform rapid, real-time detection without complex sample preparation. This is very useful for applications that require immediate results, such as biomedical testing and environmental monitoring [3].

- Non-destructive: Fluorescence detection is usually non-destructive and does not damage or alter the sample, making it suitable for analyzing valuable samples or living tissues.
- Multiplex Detection: By using different fluorescent dyes or probes, multiple target substances can be detected simultaneously. This is particularly important in biological research for complex multiparameter analysis.
- Automation and High Throughput: Modern fluorescence detection equipment can achieve automated operation and high throughput analysis, suitable for large-scale screening and analysis, especially in drug development and genetic research.
- Wide Range of Applications: Fluorescence analysis methods are widely used in various fields, including biomedicine, environmental science, materials science, and food safety [3].

In conclusion, our project has decided to use fluorescence detection methods. A key objective of our project is to detect trace contaminants in water by observing their fluorescence peaks that appear in the spectrum, and to identify substances based on the position and intensity of these peaks. The achievement of this objective relies on the high sensitivity and high selectivity of fluorescence analysis, allowing us to accurately detect and identify contaminants in complex water samples. Through this method, we aim to provide a rapid, accurate, and non-destructive means of water quality detection, applicable to environmental monitoring and public health protection [10].

Another target of our larger project was to measure the absorbance of the Ex light. This is because the fluorescence emitted by fluorescent dyes is usually of very low intensity. We need to amplify the fluorescence signal and collect as much fluorescence as possible to enhance the sensitivity of the entire system (i.e., to achieve the detection of trace contaminants in water [11]).

Absorbance measurements do not have a low intensity, but demand accurate detection and amplification of very small differences between two signals (reference light beam and the one transmitted through the sample). This can be achieved using, e.g., an instrumentation amplifier. The work for this dissertation focused on two key aspects. The first was to help the design and implementation of an optical system capable to perform both absorbance and fluorescence measurements at the same time. The second was to design an instrumentation amplifier as a high sensitivity high gain system for absorbance measurements, as it will be detailed in Chapter 4. However, for completitude, this Dissertation will also briefly provide some data regarding fluorescence measurements. Thus, Chapter 2 will review the basics of fluorescence and the main detection systems reported in Literature for this purpose. It will also briefly present signal processing methods for weak fluorescence signals, while Chapter 3 will describe an optical system that can collect most of the fluorescence emission. The same system is also designed to enable performing simultaneously the transmission/absorption measurement as well as the fluorescence one. This multidimensional analytical approach will help enhance the accuracy and reliability of water quality detection, providing scientific support for environmental protection and resource management.

1.3 Thesis Organization

The thesis is organized into five chapters. Chapter 1 presents the background of fluorescence analysis and the motivation for the water purifier design concept through fluorescence detection. Chapter 2 literature review describes the fundamentals of low light detection in recent years, including the structure, principle of operation and basic information about each circuit module. Chapter 3 simulates the model structure of this project using optical simulation and examines its advantages and disadvantages in order to compare it with conventional schemes.

Chapter 4 describes several basic methods of fluorescence detection and introduces the principle of the differential amplification circuit for weak light signals used in this project. The last chapter contains the project conclusions and recommendations for future work.

The basic structure of a fluorescence detector is shown in Figure 1.1 [12]. The detector converts light (photons) into an electronic signal in the form of an electronic charge, current, or voltage. An electronic signal in the form of an electrical charge, current, or voltage. A single photomultiplier tube or silicon photodetector is usually used.

Early use of optical methods for water quality testing instruments are mostly expensive, bulky, and only professional water quality testing departments and some government environmental protection agencies can afford the corresponding instrument use and maintenance costs, with great limitations. Therefore, in order to provide increased efficiency, portability and measurement speed at reduced cost, in the last period a lot of efforts were made to develop integrated portable water quality

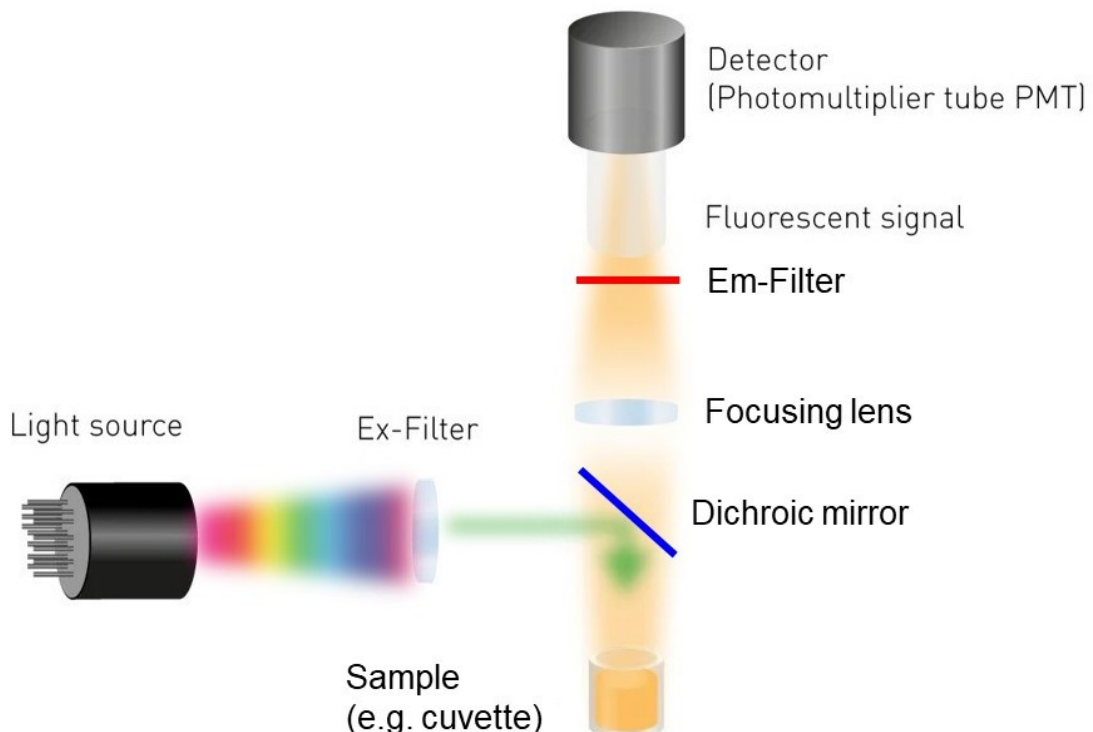


Figure 1.1: Generic fluorescence measurement setup (adapted from [12])

testing sensors which have the advantages of fast detection speed, small size, low power consumption, low price and easy to operate. Consequently, such miniaturized measurement systems can be easily used to provide relevant data for the environmental protection department to develop governance and preventive measures to provide the rationale for the basis for minimizing the impact of water pollution sources on the surrounding people and the environment, and to reduce the impact of water pollution on the environment.

Chapter 2

Literature Review

2.1 Fluorescence

2.1.1 Fundamental operation principle

Fluorescence is a physical property in which specific atoms or molecules absorb light at a specific wavelength and then emit a longer wavelength of light. The fluorescence process consists of three important stages: Excited state lifetime (Ex), and fluorescence emission (Em). The time delay from Ex to fluorescence Em is of about 1 ns, making fluorescence a good indicator for real-time observation [13]. Figure 2.1 illustrates a simple electronic state diagram (called a Jablonski diagram) corresponding to the fluorescence process [14].

During the excitation phase, the energy of a photon is introduced and absorbed by a fluorophore. Typically, an external energy source such as an incandescent lamp, UV light, or laser is used for this application [15]. Vibrational relaxation causes the fluorophore in the excited state to drop to a lower energy level in the picosecond level (S_1). During the Ex state phase, the excited molecule stays in the lowest excited singlet state (S_1) for a nanosecond and then eventually returns to the initial state. At the same time, the

fluorophore undergoes a conformational change, releasing energy to other molecules or the local environment. The final stage of the fluorescence process is called the fluorescence Em stage. An energetic photon is emitted to return the fluorophore to the ground state S_0 . This photon has a much lower energy due to energy dissipation during the excited state lifetime. Therefore, the emitted light has a longer wavelength than the Ex light ($h\nu_{EX}$) [16]. The energy difference or wavelength shift expressed by ($h\nu_{EX} - h\nu_{EM}$) is called the Stokes shift [17]. The value of the Stokes shift is crucial for fluorescence measurements because this value indicates the effect of isolation of the emitted signal from the Ex light [18].

The discrete electron leaps in Figure 2.1 are typically represented in the form of broad energy spectra called fluorescence excitation (or absorption) spectra, and fluorescence emission spectra, respectively. [19].

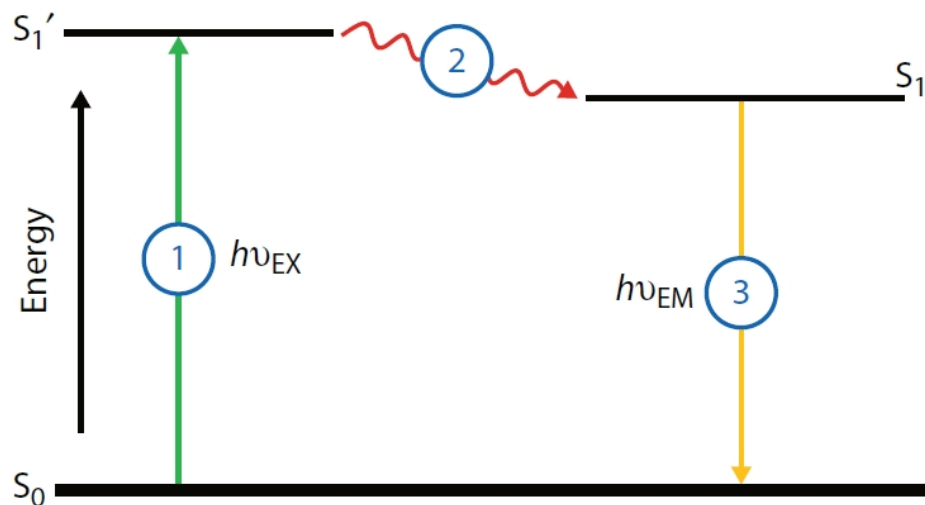


Figure 2.1: Jablonski diagram illustrating the process involved in the creation of an excited electronic singlet state in fluorescence molecules by optical absorption and subsequent fluorescent light Em (adapted from [19].)

2.1.2 Fluorescence detection principle

Fluorescent dyes have good fluorescence characteristics. The absorption spectrum represents the ability of a substance to absorb light energy at different wavelengths, showing specific peaks corresponding to electronic transitions within the molecule. Each substance has a unique absorption spectrum, making it useful for qualitative and quantitative analysis [13]. The Em spectrum represents the ability of a substance to emit light energy when returning from an excited state to the ground state, displaying fluorescence at specific wavelengths. Each substance also has a unique Em spectrum, which is particularly useful for high-sensitivity detection in fluorescence analysis [14]. By combining information from both the absorption and Em spectra, we can gain detailed insights into the optical properties of substances and design appropriate detection methods to identify and quantify trace substances [20].

The relationship between fluorescence intensity and fluorescent dye concentration is based on the Beer-Lambert law of absorption [13]:

$$I_f = \phi I (1 - 10^{-abc}) \quad (2.1)$$

Where I is the intensity of incident light, I_f is the intensity of fluorescence, c is the concentration of fluorescent dye, b is the optical length, ϵ is the molar absorption coefficient, and ϕ is the fluorescence efficiency of the fluorescent dye. When $\epsilon bc < 0.05$, Equation 2.1 can be expanded by Taylor series, and the higher order terms can be neglected:

$$I_f = 2.3\phi I \epsilon bc \quad (2.2)$$

When the fluorescent dye solution is very dilute, the fluorescence intensity has a great linear relationship with the concentration of the fluorescent dye, and the fluorescence method has the highest sensitivity.

There are two sensors and have two optical paths: fluorescence detection path and reference path, and they share the same light source shown in figure 2 .4. The luminous intensity of the light can be affected by temperature and drive current fluctuations, so a reference path was added in the sensor. Another photodiode was used to detect the light intensity scattered by the light source. The influence of fluctuation can be compensated by the intensity relationship between fluorescence and reference light.

The emitted light intensity is I_0 , and the fluorescence intensity detected by PD is I_f . The intensity of light used to excite fluorescence is $K_f I_0$, and the intensity of light entering the reference path is $K_r I_0$. Both K_f and K_r are constants and $K_f + K_r < 1$. I_f can be calculated as follows [13]:

$$I_f = 2.3\phi K_f I_0 \varepsilon b c \quad (2.3)$$

Suppose I_r is the light intensity received by the photodiode in the reference light path. It can be calculated according to eqn. (2.4) [13]:

$$I_r = K_r I_0 \quad (2.4)$$

The relationship between I_f , I_r , and c can be calculated based on eqn. (2.3) and eqn. (2.4) as follows [13]:

$$\frac{I_f}{I_r} = \frac{2.3\phi K_f I_0 \varepsilon b c}{K_r I_0} = 2.3 \frac{K_f}{K_r} \phi \varepsilon b c \quad (2.5)$$

Therefore, when the solution is very dilute, the ratio of the two light intensities is proportional to the concentration of the fluorescent dye and is not affected by light source fluctuations.

Since the intensity of fluorescence is very weak, how to amplify the extracted fluorescence signal to collect more fluorescence signal is the focus of this dissertation.

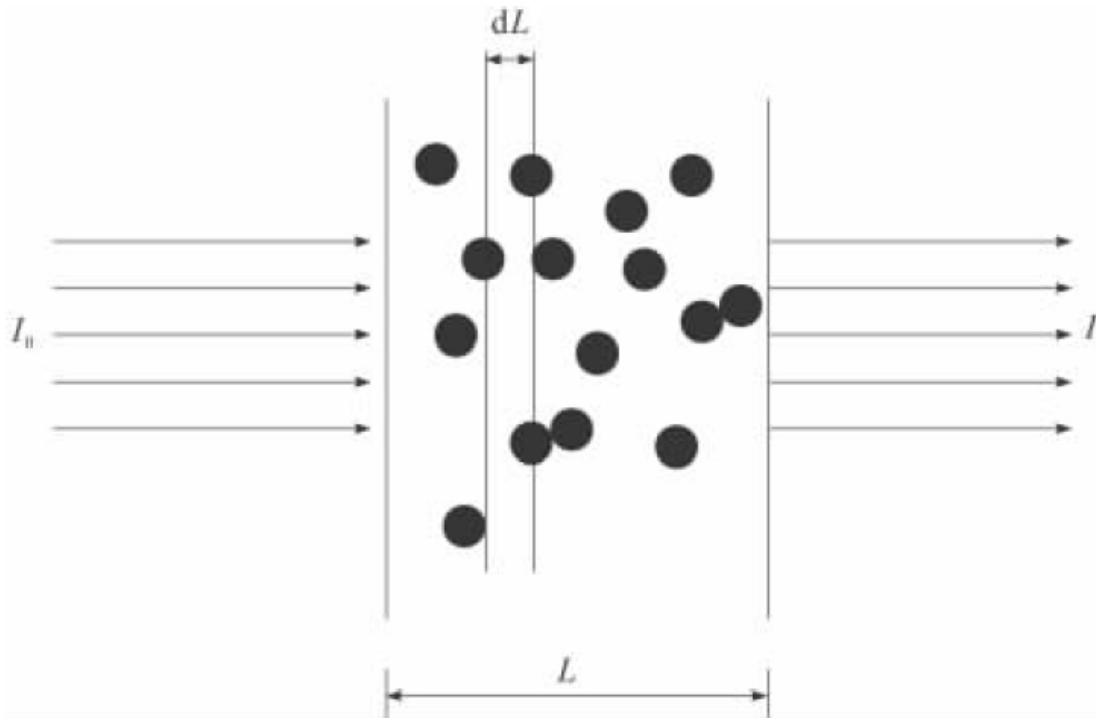


Figure 2.2: Schematic diagram of light beam passing through a sample with fluorescent molecules, represented by the black circles.

2.1.3 The principle of fluorescence concentration measurement based on the method of light transmission

During the development of fluorescence concentration measurement system based on light transmission, it is necessary to monitor the changes in the fluorescence concentration in real time. The variation in fluorescence concentration causes changes in the intensity of the transmitted light detected by the photodiode, thereby achieving the monitoring purpose. Therefore, the design of the detection circuit is related to the accuracy and sensitivity of the entire measurement system. Figure 2.2 shows a schematic diagram of the light beam passing through the fluorescence area [21].

According to the definition of the extinction cross-section, the reduced light intensity is [21]:

$$-SdI = IC_{\text{ext}} NSdL \quad (2.6)$$

where S is the scattering cross-sectional area, and C_{ext} is the extinction cross-section.

By integrating equation (2.6), we get [21]:

$$I = I_0 e^{-NC_{\text{ext}}L} \quad (2.7)$$

where I_0 is the light source provided by the laser, and I is the transmitted light received by the photodetector. The change in the measured fluorescence concentration will inevitably cause changes in the intensity of the transmitted light, and the light signal received by the photodetector will also change accordingly.

Through analysis and research, if a simple transmission method is used for measurement, once the power supply of the laser light source is unstable or the temperature of the laser light source changes, it will cause changes in the incident light intensity I_0 of the laser light source. At this time, even if the fluorescence concentration in the measured area does not change, the transmitted light intensity I will change, and the changed signal received by the photodetector will be incorrect information, which will lead to errors in the measurement results and inaccurate data.

Therefore, the measurement system adopts the differential measurement method with dual-beam detection. At the emission end, a beam splitter is used to split the laser beam into two beams. One beam directly passes through the beam splitter into the measured area and is then detected by the detection photodetector to measure the transmitted light intensity I . The other beam is used as the reference light I'_0 and is directly sent to the reference photodetector. Finally, a differential amplifier is used to perform differential operations on the signals input by the reference photodetector and the detection photodetector. Assuming that the fluorescence concentration in the measured area remains un-changed, if the incident light intensity I_0 of the measurement system changes due to instability of the power supply of the laser light source or temperature changes of the laser diode (ΔT) [21], the transmitted light and reference light will undergo the same magnitude of change because they are split from the same beam. Therefore, the differential value will still not change. This not only reduces the measurement error caused by the instability of

the light source but also overcomes the interference of background light during the measurement process.

In the simple transmission measurement principle, if the light source is stable, the transmitted light intensity will change with the variation of the measured fluorescence concentration. By using fluorescence concentration calibration technology, the one-to-one correspondence between the transmitted light intensity and the fluorescence concentration can be determined. When using the differential detection structure for measurement, the concentration of the measured fluorescence will correspond one-to-one with the difference between the signals of the detection photodetector and the reference photodetector, which can also be determined using calibration technology.

2.1.4 Traditional fluorescence detection

High sensitivity detection in microfluidic systems has several advantages [22]:

- Obtain accurate two-dimensional images of fluorescence distribution for image analysis.
- Low detection limit, high stability, good spatial resolution and excellent discrimination capability.

To achieve high-resolution in a fluorescence detection system, it includes an Ex filter, a dichroic mirror, and a blocking filter. In a typical fluorescence microscope, a filter combination is used to select specific desired Ex and Em wavelengths. Figure 2.3 describes the basic setup of a fluorescence microscope. The Ex filters transmits only the specific wavelength at which absorption in the fluorophore peaks. The blocking

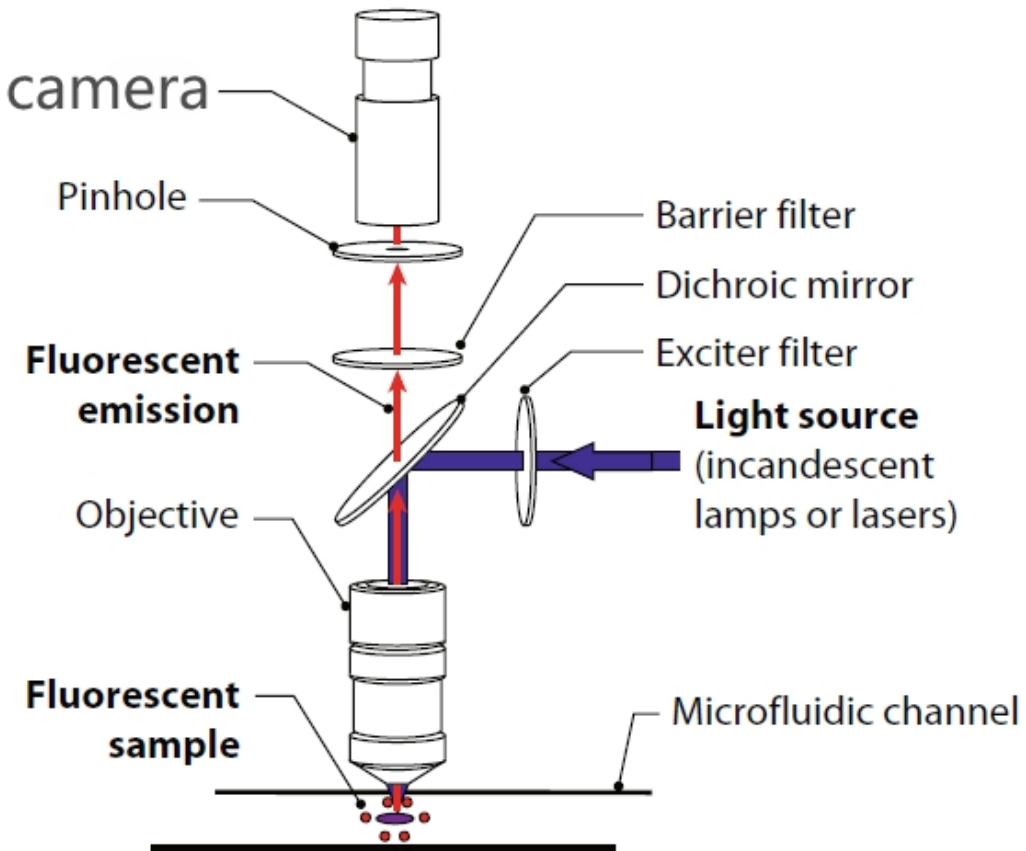


Figure 2.3: Traditional fluorescence microscopy configuration for high sensitivity detection (adapted from [21]).

filter suppresses Ex wavelengths and transmits only longer Em wavelengths to the detector. The dichroic mirror is specifically designed to effectively reflect Ex wavelength and transmit the Em wavelengths. This optical system needs to be carefully tuned in order to optimize various parameters such as pinhole size, channel depth, Ex efficiency size, Ex efficiency, and laser spot size, among various other parameters. This fluorescence system is capable of achieving very low detectable fluorophore concentrations by carefully adjusting and optimizing various parameters, such as pinhole size, channel depth, Ex efficiency, and laser spot size. Detectable concentrations of fluorescein can be as low as 300 fM [22].

There also exists a need for compact, portable, and simple fluorescence detection systems for on-site, point-of-care diagnostic applications that do not necessarily require the precise information of spatial fluorescence distribution.

2.1.5 Optical spatial filters

In order to excite and detect fluorescence without interfering with the Ex and Em spectra of the fluorophore, optical spatial filters are essential for fluorescence detection as shown in Figure 2.3. The drawback of the Ex filter is that it reduces the intensity of the Ex light reaching the detector. The lower the Ex light intensity, the weaker the detected intensity of the emitted fluorescence. This is a challenge because the intensity of the Ex light is typically several orders of magnitude higher than the intensity of the fluorescence signal. In recent years, advances in optical filtering technology have produced several devices with superior performance over conventional absorption or interference filters. Liquid crystal and acousto-optic devices have been developed for wavelength selection via electronically controlled systems called tunable filters. Typical wavelength-selective liquid crystal selective liquid crystal tunable filters are constructed by stacking various liquid crystal layers with linear polarizers.

2.2 Examples of reported fluorescence detection systems

The next sections present the main types of traditional fluorescence systems that are widely used in biomedical applications and analytical chemistry.

2.2.1 LED-Based Fluorescence Detection System

- **Structure:** This system, shown in Fig.2.4, typically includes a LED light source, lenses, interference filters, a dichroic mirror, an objective lens, a capillary flow cell, a photomultiplier tube (PMT), and a computer interface. The light emitted by the LED is focused through a series of optical components and illuminates the sample. The fluorescence signal is collected by the objective lens and transmitted through filters and lenses to the PMT [23].

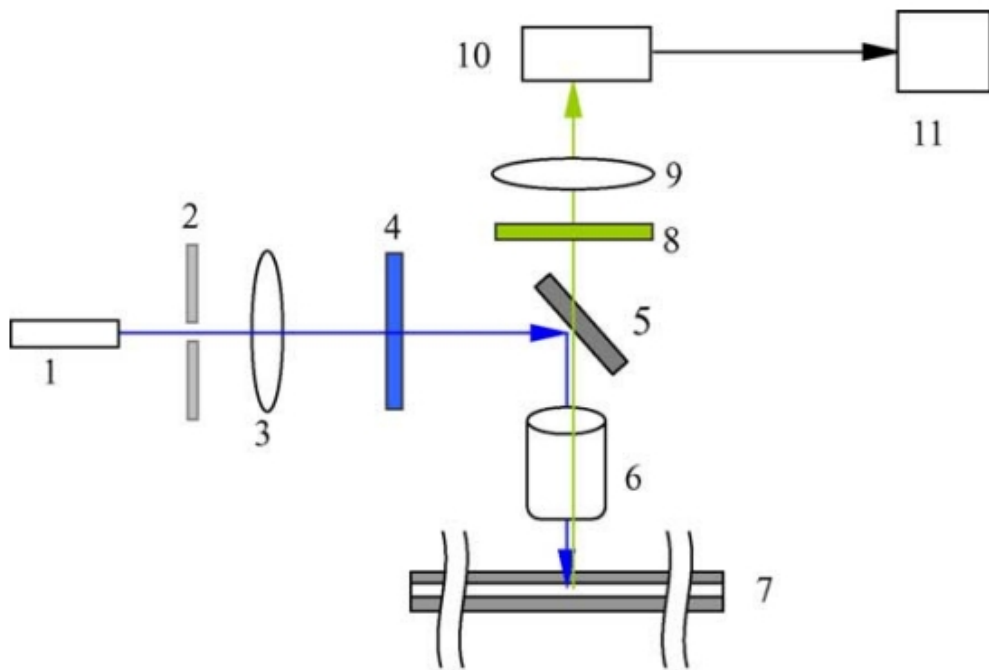


Figure 2.4: Schematic diagram of LED-induced fluorescence detection system: (1) LED; (2) iris; (3) lens (focal length 6 cm); (4), interference filter (BP 470 nm); (5) dichroic mirror; (6) objective; (7) capillary flow cell; (8) interfere filter (BP 530 nm); (9) lens (focal length 6 cm); (10) photomultiplier tube (PMT); (11) personal computer (adapted from [22])

- **Advantages:**

- Compact structure and easy integration
- Low cost and durable
- High stability and convenient light intensity adjustment
- Long lifespan

- **Disadvantages:**

- Large divergence angle, difficult to focus
- High background noise, lower detection sensitivity
- Requires precise optical alignment, complex operation

Such a reported system achieved excellent performance characteristics. Its limit of detection (LOD) for FITC-labeled phenylalanine was 10 nM without preconcentration (signal-to-noise ratio of 3). With preconcentration techniques, the LOD was further reduced to 1 nM or less. The detector shows a good linear response in the concentration range of 1×10^{-7} M to 2×10^{-5} M with $R^2 = 0.999$. In fluorescence detection, the use of a 470 nm high-brightness LED as the Ex source in this collinear scheme effectively reduced the interference of Ex light and background levels [23]. This system is suitable for routine analysis of proteins, peptides, amino acids, and other compounds when combined with capillary electrophoresis (CE), high-performance liquid chromatography (HPLC), or flow-injection analysis (FIA).

2.2.2 Laser-Induced Fluorescence Detection System (LIF)

- **Structure:** A LIF system, as the one shown in Fig.2.5, uses a laser as the light source to excite fluorescent molecules. The system includes a laser, optical filters, optical fibers or lenses, a detection cell, and a detector (usually PMT or CCD). The laser light is focused through filters onto the sample, and the resulting fluorescence signal is collected and detected [24].
- **Advantages:**
 - High monochromaticity and light intensity;
 - High detection sensitivity and low background noise;
 - Suitable for high-precision quantitative analysis.
- **Disadvantages:**
 - High equipment cost.
 - Large size and high power consumption
 - Limited lifespan of the light source, frequent replacement required

The specific compact and highly sensitive light-emitting diode-induced fluorescence detector (LED-FD) reported in literature that is shown in Fig.2.5 exhibited notable performance characteristics: a LOD for sodium fluorescein of 0.75 nM with a SNR of 3. This represents a 3.5-fold enhancement in SNR compared to

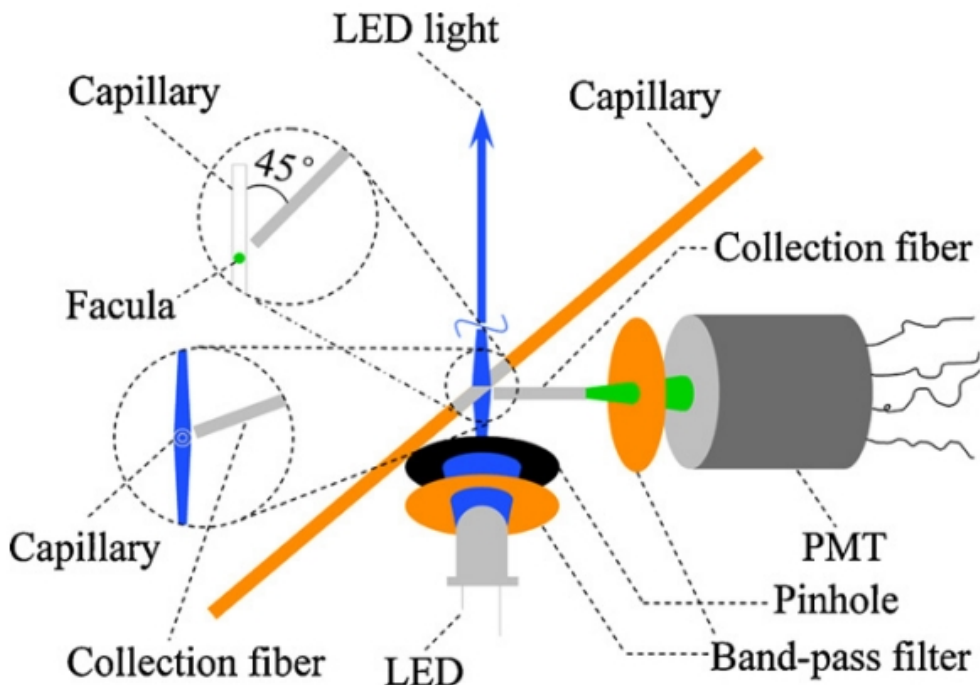


Figure 2.5: Schematic diagram of the optical setup of the LED-FD system (adapted from [23]).

previous designs. The detector demonstrated a linear response in the concentration range of 2–200 nM with an R^2 value of 0.9993. The repeatability error was within 2% relative standard deviation (RSD) on peak height for ten repeated injections of a 5 nM solution, and the reproducibility between devices was within 2.2% RSD for a 10 nM fluorescein solution [24]. The use of a 470 nm high-brightness LED as the Ex source effectively minimizes interference and background levels. This setup ensures optimal performance for routine analysis of proteins, peptides, amino acids, and other compounds when combined with capillary electrophoresis (CE), high-performance liquid chromatography (HPLC), or flow-injection analysis (FIA).

2.2.3 Time-Resolved Fluorescence Immunoassay (TRFIA)

- **Structure:** A TRFIA system (Fig.2.6) typically includes a UV LED light source, narrow-band optical filters, a silicon photodiode (Si PIN), amplifiers, an analog-to-digital converter (ADC), and a microcontroller [25].

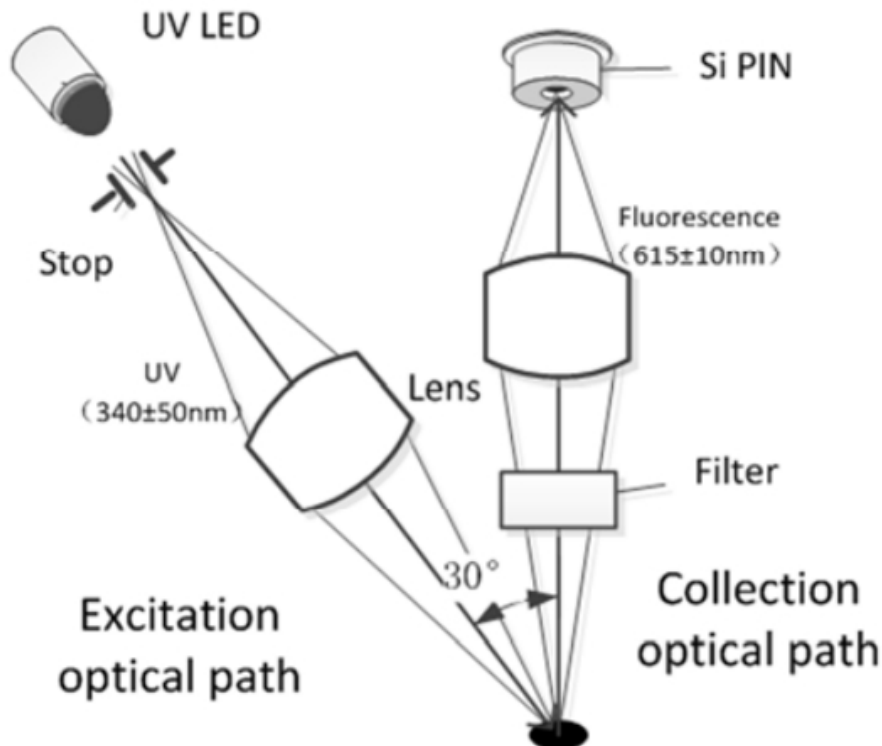


Figure 2.6: An example of a TRFIA system (adapted from [24]).

- **Advantages:**

- High specificity and sensitivity, suitable for detecting various antibodies and bioactive substances
- Time-resolved technology effectively reduces background fluorescence interference, improving detection accuracy
- Suitable for point-of-care testing (POCT), compact equipment size

- **Disadvantages:**

- Complex technology requiring high precision time control
- The choice of light source and detector needs precise matching
- Relatively high cost

The light-emitting diode-induced fluorescence detector (LED-FD) shown in Fig. 2.6 exhibited notable performance characteristics: an LOD of 19 nM for FITC-labeled phenylalanine without preconcentration and a SNR of 3. With preconcentration techniques, the LOD can be further reduced to 1 nM or

less. The detector had good linear response in the concentration range of 10^{-7} M to 2×10^{-5} M with $R^2 = 0.999$ [25].

2.2.4 Conclusion

The advantages and disadvantages of these three conventional fluorescence detection systems were described in the previous sections. The advantages are very sensitive (low LOD), high stability, good spatial resolution, excellent discrimination capability. The disadvantages are very complex and bulky system, with microscope typically needed for imaging and ensuring the mentioned spatial resolution and discrimination capabilities. Also, miniaturization is difficult, typically with some loss of performance. Therefore one of our main aims was to design and implement a simple proof-of-concept of a small novel system for the desired UVA/T water analysis used for membrane integrity monitoring. Such a system will be described later, in Chapter 3 and Chapter 4.

2.3 Weak signal detection methods

2.3.1 Background

No matter whether in daily life or in fluorescence detection applications, noise signals are ubiquitous. They often mix with useful signals and overshadow them, making it difficult to separate the noise from the useful signals using conventional methods, which severely restricts the normal operation of systems and affects the quality of useful signals. In the field of signal processing, it is generally necessary to suppress or eliminate noise to obtain useful signals. For weak signals, compared to strong signals, detection is more difficult, and the signal-to-noise ratio is much lower [26].

Weak signal detection includes measurement of both physical and electrical parameters. All physical quantities can be converted into electrical quantities, such as voltage, current, and flow. Weak signal detection relates to very low detection levels.

For example, the voltage measurement range is from 10^{-10} to 10^{-6} μ V, the current measurement lower limit is from 10^{-5} to 0.1 nA, the weak light detection range is from 10^{-17} to 10^{-13} W/cm², and the electric field measurement range is from 10^{-5} to 10^{-1} pF. If the signal-to-noise ratio (SNR) is improved, conventional detection technology can achieve an SNR of 10, while weak signal detection technology can achieve an SNR of up to 10,000 times or even higher [27].

In 1928, Johnson conducted research on the noise generated by the thermal motion of electrons, laying the foundation for weak signal detection. Many scientists have since made outstanding contributions to the field of weak signal detection. In the past few decades, the development of this technology has been rapid and aggressive, continuously pushing the limits of weak signal detection and noise reduction. In 1962, the first commercial lock-in amplifier was developed at the PARC research institute in the United States, improving the signal-to-noise ratio of weak signal detection by a factor of 10^3 [28]. In 1968, Auger electrons (secondary electrons emitted by atoms when their electrons are excited) were detected from a large background of secondary electrons; in the early 1980s, under specific conditions, the noise ratio of weak signal detection was improved by a factor of 10^6 , enabling the detection of signals with an amplitude of less than 1 nV and obtaining high-precision signal outputs, with a high precision signal amplification of up to 200 dB [29]. With the rapid development of science and technology, it is now possible to detect micro-phenomena or weak signals that were previously undetectable. This has propelled the development of multiple disciplines such as physics, geophysics, astronomy, and electrophysiology, as well as biology, and has also promoted the comprehensive development of engineering technology fields. At the same time, weak signal detection technology has become a highly regarded new interdisciplinary field [30].

2.3.2 Correlation Detection

Correlation detection, as a technical discipline based on stochastic processes and information theory, fundamentally involves measuring the correlation of two time-domain signals. Correlation detection has demonstrated relatively superior performance in weak signal detection and has been widely applied in fields such as communication, optics, acoustics, automatic control, and mechanical vibration analysis [31].

Through previous studies, it has been found that useful signals are periodic, while noise is random and uncorrelated. Correlation detection uses this distinction to perform related operations on the useful signal with the reference signal that has the same period and phase as the useful signal, thereby suppressing noise. The measurement of the useful signal is based on the correlation of the two signals. The noise is random and uncorrelated with the reference signal, so it does not affect the measurement results [32].

Correlation detection is essentially a method to extract useful signals from a noisy environment by correlating the received signal with a reference signal, thereby eliminating noise. The key concept of correlation detection is to measure the correlation between two signals in the time domain. If the two signals are correlated, the noise can be effectively filtered out, and the useful signal can be enhanced [33].

The basic idea of correlation detection is to use a reference signal that has the same frequency and phase as the useful signal to perform correlation operations on the received signal, thus eliminating noise. This method has been widely used in weak signal detection, achieving high-efficiency noise suppression and significantly enhancing the detection of weak signals [34].

The theoretical basis of autocorrelation is the dependency of the same signal on different time points. The principle of autocorrelation detection of signals is shown in Figure 2.7, where the signal to be measured is $s(t)$, the noise

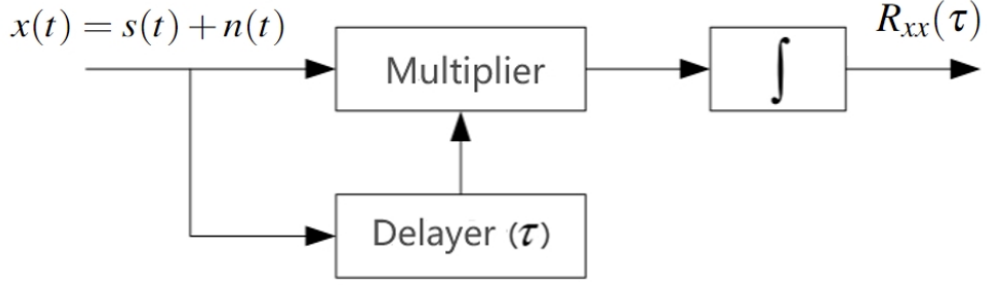


Figure 2.7: Block diagram of the autocorrelation detection method [33].

signal is $n(t)$, and the input signal $x(t)$ consists of $s(t)$ and $n(t)$. Thus, the input signal can be expressed as $x(t) = s(t) + n(t)$. Then, the delayed input signal $x(t - \tau)$ is fed into a multiplier to perform the correlation operation. The averaged value of the correlated signal is obtained by the integrator, thereby getting the autocorrelation value of $x(t)$. By changing the delay time τ , the autocorrelation detection calculation is performed, so that the autocorrelation function can be expressed as a function of the delay time τ .

The expression for the auto-correlation function can be obtained as [34]:

$$R_{xx}(\tau) = \lim_{T \rightarrow \infty} \frac{1}{T} \int_{-T/2}^{T/2} x(t)x(t - \tau) dt = R_{ss}(\tau) + R_{sn}(\tau) + R_{ns}(\tau) + R_{nn}(\tau) \quad (2.8)$$

In eqn. (2.6), since the measured signal $s(t)$ and the noise signal $n(t)$ are not related, the values of the cross-correlation functions $R_{sn}(\tau)$ and $R_{ns}(\tau)$ are generally zero. Therefore, the value of the autocorrelation function $R_{xx}(\tau)$ is equal to $R_{ss}(\tau)$, which means the input signal's autocorrelation function can be simplified to [34]:

$$R_{xx}(\tau) = R_{ss}(\tau) + R_{nn}(\tau) \approx R_{ss}(\tau) \quad (2.9)$$

Auto-correlation detection is performed on the same signal, whereas cross-correlation detection is performed on different signals. The principle of cross-correlation detection is shown in Figure 2.8.

As shown in Figure 2.8, the input signal is split into two paths, $x(t)$ and $y(t)$. Here, $x(t)$ is the mixed signal of the signal to be measured $s(t)$ and the noise signal $n(t)$, and $y(t)$ is the reference signal synchronized with the

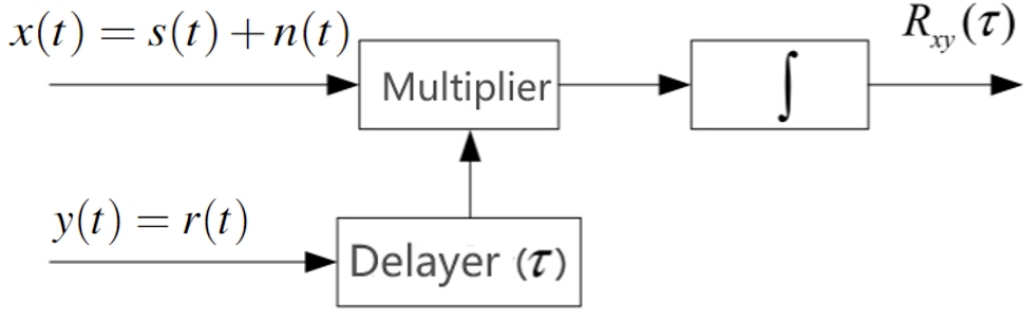


Figure 2.8: Block diagram of the cross-correlation detection method [33].

measured signal. Assuming $y(t) = r(t)$, according to the fact that the measured signal $s(t)$ and the reference signal $r(t)$ are synchronous and correlated, while the noise $n(t)$ and the reference signal $r(t)$ are random and uncorrelated. The cross-correlation function is given by [33]:

$$R_{xy}(\tau) = \lim_{T \rightarrow \infty} \frac{1}{T} \int_{-T/2}^{T/2} x(t)y(t - \tau)dt = R_{sr}(\tau) + R_{nr}(\tau) = R_{sr}(\tau) \quad (2.10)$$

The autocorrelation function $R_{xx}(\tau)$ can be expressed as:

$$R_{xx}(\tau) = E[x(t) \cdot x(t + \tau)] \quad (2.11)$$

Expanding this, we get:

$$R_{xx}(\tau) = R_{ss}(\tau) + R_{sn}(\tau) + R_{ns}(\tau) + R_{nn}(\tau) \quad (2.12)$$

where $R_{ss}(\tau)$ is the autocorrelation of the signal, $R_{nn}(\tau)$ is the autocorrelation of the noise, and $R_{sn}(\tau)$ and $R_{ns}(\tau)$ are the cross-terms between the signal and noise.

The cross-correlation function $R_{xy}(\tau)$ can be expressed as [33]:

$$R_{xy}(\tau) = E[x(t) \cdot y(t + \tau)] \quad (2.13)$$

where $y(t)$ is the reference signal. Assuming the reference signal is noise-free (i.e., $y(t) = s(t)$), we get [33]:

$$R_{xy}(\tau) = R_{ss}(\tau) + R_{ns}(\tau) \quad (2.14)$$

Since $R_{ns}(\tau)$ is usually very small or negligible, the cross-correlation function primarily consists of the signal correlation $R_{ss}(\tau)$, and the noise component is significantly reduced. By comparing the autocorrelation eqn. (2.10) with that for cross-correlation (2.8), By comparing the formulas for autocorrelation and cross-correlation, it can be seen that the autocorrelation function includes all the combined terms of both signal and noise, whereas the influence of noise is minimized in the cross-correlation function. Therefore, the output after cross-correlation is less noisy than the output after autocorrelation. This is why cross-correlation is often considered a more effective method than autocorrelation in signal processing, especially in noise reduction [31].

2.3.3 Lock-in amplifier

Lock-in amplification is a very common method in weak signal detection, which can effectively separate the useful signal from noise. A sinusoidal signal is used to modulate the Ex light source, and, hence, the intensity of the transmitted or fluoresced light which will provide (after photodetection) the input signal into the system. At the same time, a sinusoidal reference signal, with the same frequency and phase as the response signal (obtained from the initial Ex light beam after a beam splitter, see Fig.3.10 in next Chapter), is used to demodulate the weak input signal, filtering only one of the modulation components with high selectivity by using a very narrow pass-band filter with a very high quality factor [28]. The block diagram of a lock-in amplifier is shown in Figure 2.9.

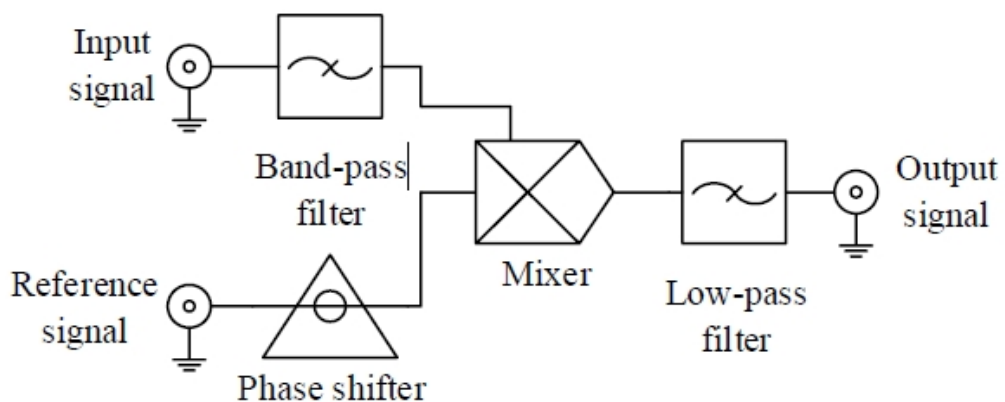


Figure 2.9: Block diagram of a lock-in amplifier.

The operating principle of lock-in amplification relies on the use of a reference signal $V_r(t)$ with the same frequency as the input signal $V_s(t)$ [35]:

$$V_r(t) = \sqrt{2} \cos(\omega_r t) \quad (2.15)$$

The input signal $V_s(t)$ is given by:

$$V_s(t) = R \cos(\omega_s t + \theta) \quad (2.16)$$

The lock-in amplifier multiplies the input signal by the reference signal:

$$V_s(t) \cdot V_r(t) = R \cos(\omega_s t + \theta) \cdot \sqrt{2} \cos(\omega_r t) \quad (2.17)$$

Using trigonometric identities, this can be expanded as:

$$V_s(t) \cdot V_r(t) = R \{\cos[(\omega_s - \omega_r)t + \theta] + \cos[(\omega_s + \omega_r)t + \theta]\} \quad (2.18)$$

After passing through a low-pass filter, the high-frequency component $\cos((\omega_s + \omega_r)t + \theta)$ is removed, leaving:

$$V_{\text{out}}(t) = R \cos[(\omega_s - \omega_r)t + \theta] \quad (2.19)$$

For the special case where $\omega_s = \omega_r$, the output signal simplifies to:

$$V_{\text{out}}(t) = R \cos(\theta) \quad (2.20)$$

In a dual-phase lock-in amplifier, the signal is also multiplied by a 90-degree phase-shifted reference signal $V_{r,90}(t) = \sqrt{2} \sin(\omega_r t)$, yielding the quadrature component:

$$Y = R \sin(\theta) \quad (2.21)$$

The in-phase component X and quadrature component Y can then be used to compute the amplitude R and phase θ of the input signal [35]:

$$R = \sqrt{X^2 + Y^2} \quad (2.22)$$

$$\theta = \tan^{-1} \left(\frac{Y}{X} \right) \quad (2.23)$$

Using a modulator to shift the original signal to the modulation frequency ω_0 , and then performing amplification, one can effectively avoid the impact of 1/f noise and C drift. By following this with a bandpass filter to remove noise, demodulation, and low-pass filtering, a low-noise amplified signal can be obtained. As was shown in Figure 2.9 a lock-in amplifier comprises a signal channel, a reference channel, a phase-sensitive detector (PSD), and a low-pass filter (LPF). The working process is as follows: a local oscillator generates a reference signal with the same frequency as the target signal. The reference signal is phase-shifted and is then multiplied with the input signal. The original signal contains noise, and only the components with the same frequency as the reference signal will be converted into a DC signal and then pass through the low-pass filter while all other frequency components are filtered out. Consequently, this method isolates from the noise the useful signal related to the reference signal, thus effectively suppressing the noise and improving the signal-to-noise ratio (SNR).

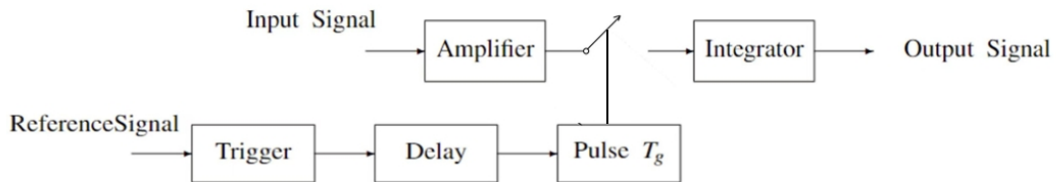


Figure 2.10: Block diagram of a sampling integration process [35].

2.3.4 Sampling Integration

The sampling integration method is commonly used to detect pulse signals submerged in noise. The sampling integrator consists of a sampler and an integrator. When the input signal is a periodic signal and is sampled at the phase position synchronized with the reference periodic signal, the multiple sampled signals are integrated. Each sampling adds positive and negative random noise, and through multiple samplings, the useful signal amplitude continuously increases while the noise amplitude continuously decreases, thereby achieving noise filtering [36].

The sampling integration process includes two continuous stages: sampling and integration. To recover weak signals submerged in noise, each signal period is divided into several time intervals, and signals within these intervals are sampled and integrated at points corresponding to the same phase position in different periods. This integration process is usually simulated by electronic circuits. The basic principle is shown in Figure 2-9. The measured signal $s(t)$, which has added noise $n(t)$, with a period T , will be input to the sampling switch K after passing through the amplifier. The measured signal is the reference signal $r(t)$ of the signal frequency, which is also the measured signal itself. The trigger circuit generates a trigger pulse signal with a certain width T_e after the reference signal waveform of the measured data is delayed, controlling the switch K to sample the input signal $x(t)$.

2.3.5 Noise filtering

This is achieved using a filter to separate the useful signal from the noise based on the frequency characteristics of the useful signal. Only signals in the desired passband pass through, while significantly attenuating or completely suppressing signals in the stop-band. Hence, filtering is an effective means of suppressing noise and improving the SNR [37].

2.3.6 Adaptive Noise Cancellation

The purpose of adaptive noise cancellation is to improve the signal-to-noise ratio during signal transmission or detection. It aims to suppress noise in signal processing by utilizing the uncorrelated characteristics of noise and the target signal. Adaptive adjustment of the adaptive filter's transmission characteristics is used to separate the target signal and suppress noise as much as possible. Adaptive filters commonly use optimization algorithms, which include statistical detection criteria, maximum signal-to-noise ratio criteria, minimum mean square error (MSE) criteria, least squares (LS) criteria, and other optimization criteria. Different adaptive algorithms are determined by different criterion functions [38].

2.3.7 Photon Counting

Photon counting is an instrument specifically used for measuring very weak light signals. With the rapid development of modern high-tech, the further application of weak signal detection in biology, physics, and chemistry has become increasingly important. Photon counting has emerged as an independent branch of weak signal detection, gaining significant support from researchers and experts in various fields. For the measurement of extremely weak light signals, photon counting instruments have become indispensable tools. Photon counting uses a digital method of accumulating and integrating the signal, allowing for the extension of integration time to improve the SNR, thereby achieving the highest possible SNR for very weak signals [39].

2.3.8 Instrumentation Amplifier

In this dissertation, an instrumentation amplifier will be used for signal amplification. This amplifier is chosen due to its high common-mode rejection ratio (CMRR), low noise performance, and high input impedance. These features make it ideal for amplifying weak photoelectric signals accurately and efficiently. The detailed implementation of the instrumentation amplifier and its role in the detection system are discussed in Chapter 4. This choice enhances the system's ability to detect weak signals, ensuring high sensitivity and precision in measurements.

Chapter 3

Optical System

3.1 Optical System Simulation

Fluorescence intensity is inherently very weak and radiated isotropically in all directions. Traditional fluorescence detection systems capture only a portion of this emitted light, which significantly limits their efficiency. To achieve higher efficiency, it is absolutely vital to collect as much of the fluoresced light as possible, ideally all of it. The proposed solution is to implement the concept of an integrating sphere, a system that functions akin to a "black-body" capturing device. An integrating sphere can collect nearly all the emitted fluorescence light, irrespective of the direction in which it is radiated. This approach maximizes the detection efficiency and improves the overall performance of the fluorescence detection system.

3.1.1 Integrating Sphere Simulated model

Solidworks was used to build the model. The diameter of the sphere is 100 mm, with two circular openings each with a radius of 5 mm. The beam from the light source is focused on the sample in the integrating sphere to excite the fluorescence emission in Figure 3.1. Both the incident light and fluorescence emission co-exist and are reflected inside the sphere. Part of the incident light beam will hit the sample and part of it will continue to bounce back and forth and excite the sample.

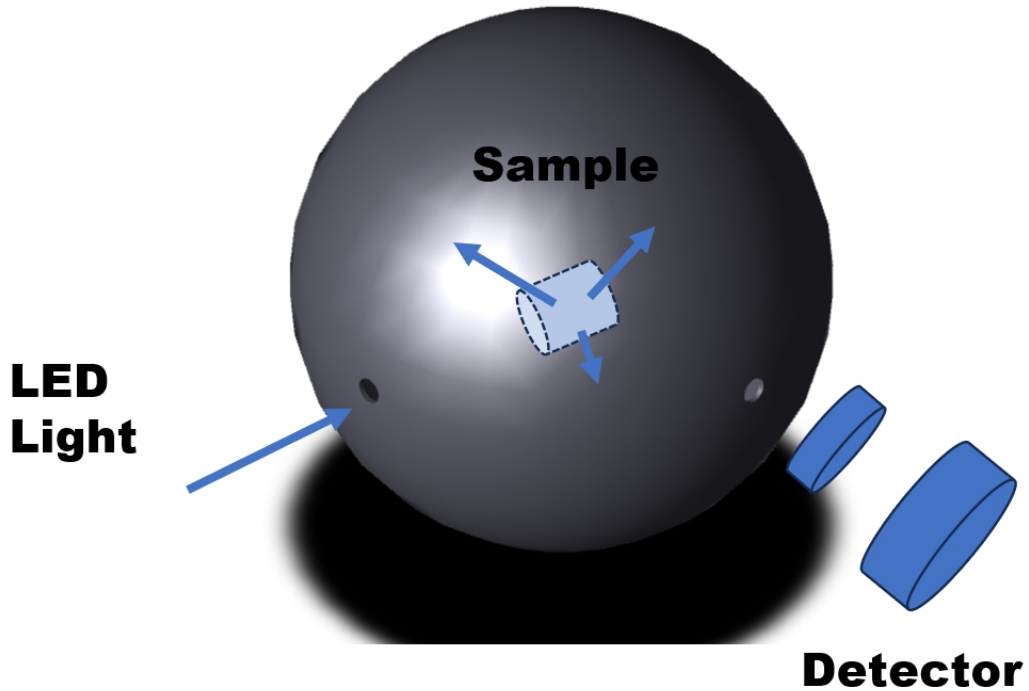


Figure 3.1: Integrating sphere model for fluorescence measurement.

3.1.2 Mathematical Derivation

Given a uniform radiation source with radiative power P and radius R , we aim to derive the resulting energy density E at a distance r .

Assume that the isotropically emitting light source is inside and at the centre of perfectly reflecting sphere. The power per unit area P_{unit} on the inner surface of the sphere is given by:

$$P_{\text{unit}} = \frac{P}{4\pi R^2} \quad (3.1)$$

Considering a small area element dA_i on the inner surface, the radiative energy density E_i is:

$$E_i = I \cos \theta \quad (3.2)$$

where $I = \frac{P_{\text{unit}}}{A_i} = \frac{P}{4\pi R^2} \cdot \frac{1}{A_i}$ and $\cos \theta = 1$. The differential energy density dE_i is:

$$dE_i = \frac{P}{4\pi R^2} \cos \theta dA_i \quad (3.3)$$

For area element dA_i , the multiple reflections result in

$$E_i = \frac{P}{4\pi R^2} \sum_{i=1}^{\infty} \cos \theta_i \quad (3.4)$$

If we consider the angle θ uniformly, and the reflections in a perfectly reflecting sphere, we can sum the contributions as:

$$E_{\text{total}} = E_1 + E_2 + E_3 + \dots = E_1 \sum_{i=1}^{\infty} \cos \theta_i \quad (3.5)$$

Thus, the total energy density becomes:

$$E = \frac{P}{4\pi R^2} \cdot \frac{1}{1 - \cos \theta} \quad (3.6)$$

$$E_{\text{total}} = E_1 + E_1 p + E_1 p^2 + E_1 p^3 + \dots = \frac{E_1}{1 - p} \quad (3.7),$$

where the variable p represents the diffuse reflectance of aluminum inside the internal cavity.; E represents the radiation illuminance.

$$\text{Radiation illuminance} = \frac{\text{Radiation Power}}{\text{Area}} \quad (3.8)$$

3.1.3 Zemax Simulations

In accordance with the dimensions provided in section 3.1.1, a solid-state integrating sphere model was imported into Zemax. The incident light power was set to 2 W, and the inner surface of the sphere was specified as aluminum. The inner surface of the optical cavity was defined as aluminum. See the coating file settings in the table below, where 0.7 is the refractive index; -7.0 is the extinction coefficient. In ZEMAX, an absorbing material is indicated when the extinction coefficient is negative, as shown in Figure 3.2.

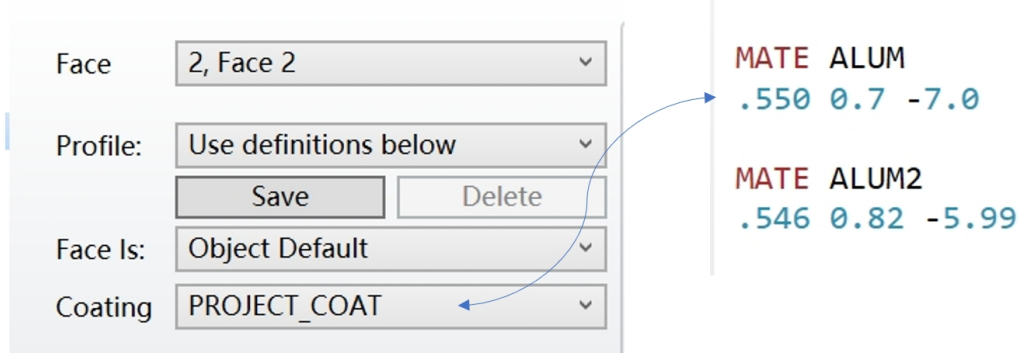


Figure 3.2: Surface coating setting in Zemax as aluminum material

A fluorescent sample was placed at the center of the integrating sphere and a surface detector was positioned at one of the apertures to measure the intensity of the fluorescence, as shown in Figures 3.3 and 3.4.

The center contains a rectangular fluorescent simulation sample and the properties of the rectangular object were set to Phosphors and Fluorescence. The absorption spectrum and emission spectrum files were then imported into Zemax. The specific parameters are as shown in Figure 3.5.

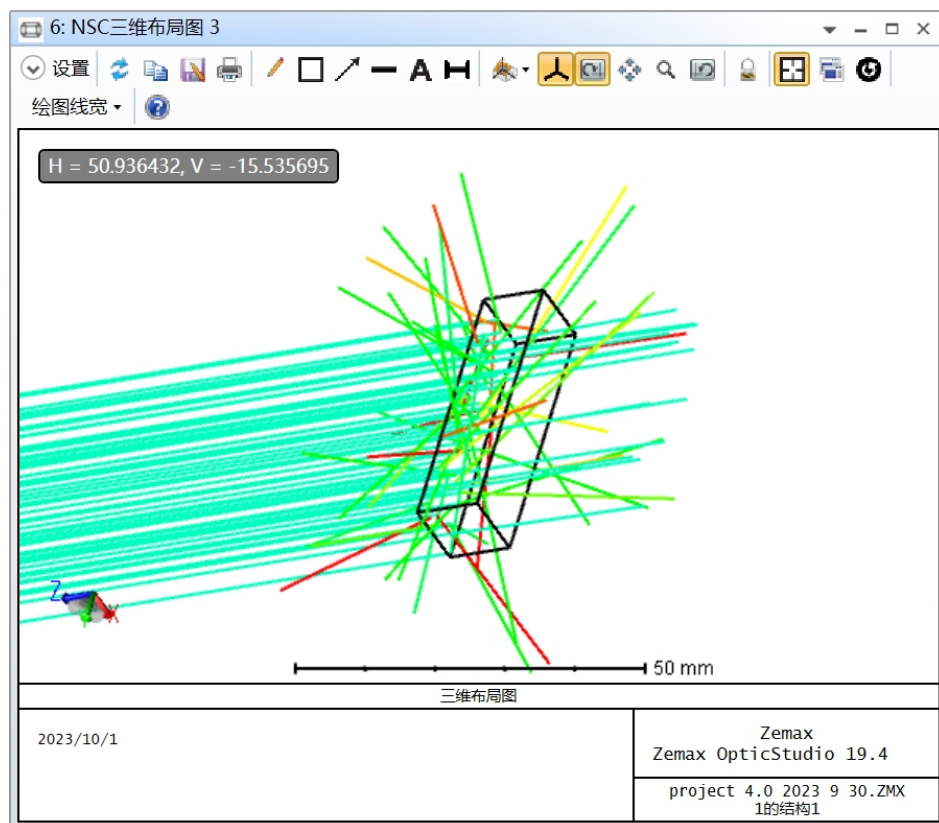


Figure 3.3: Fluorescent sample emission simulated in ZEMAX.

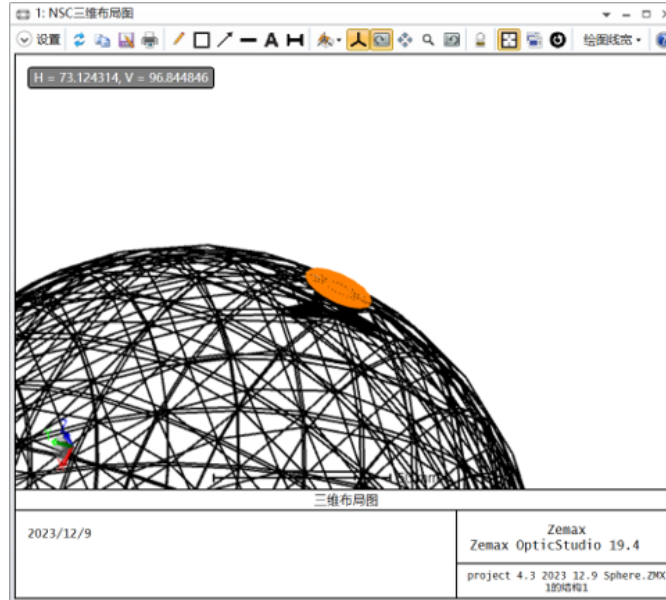


Figure 3.4: Output detector defined in ZEMAX.

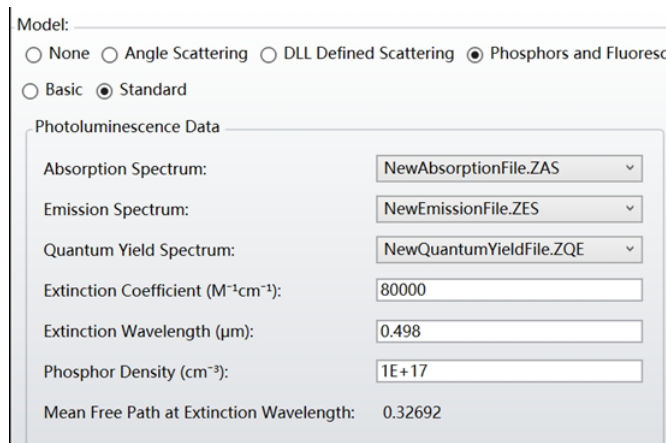


Figure 3.5: Fluorescent material model defined in ZEMAX.

3.1.4 Results

Thus, in our ZEMAX simulations we imported the spectral data of fluorescein, set up ZAS, ZES, ZQE files, and established the absorption emission, and quantum effect spectra of fluorescein, for which the excitation wavelength is 498 nm and the emission wavelength is 517 nm. The fluorescent sample in this model was a rectangular body with a length and width of 10 mm each and a height of 40 mm.

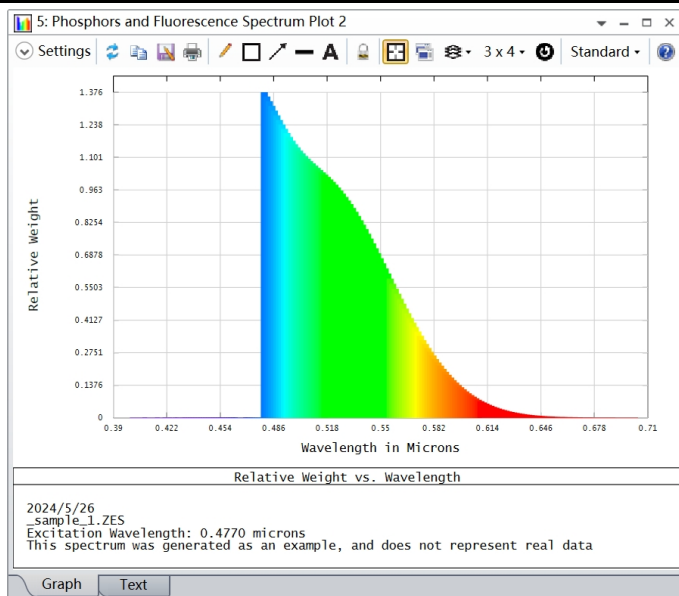


Figure 3.6: The simulated emission spectrum (Excitation wavelength = 477 nm)

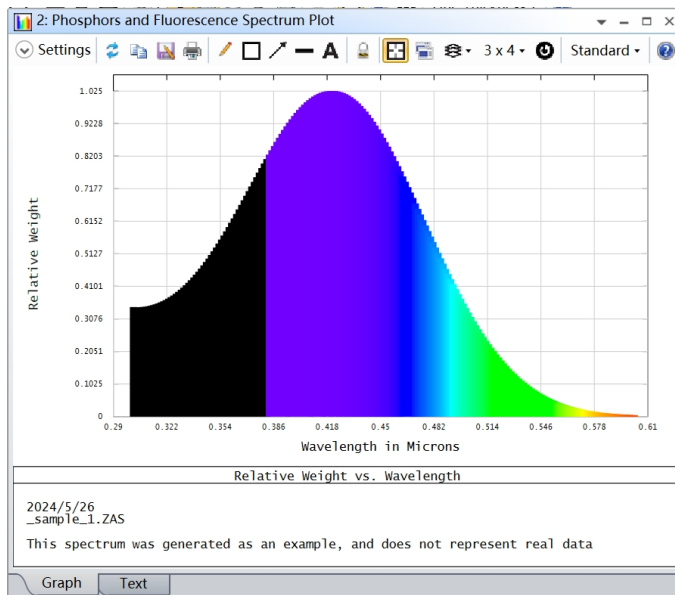


Figure 3.7: The simulated absorption spectrum (peak wavelength = 421.6 nm)

Because fluorescence is isotropic, the light emitted by the sample is divergent in all directions, although the incident light is a collimated light incident. The simulated light emitted by fluorescein is consistent with the spectral data: most of the light is in the blue-green range of the visible spectrum. Figure 3.6 shows the emission spectrum simulated in Zemax with an excitation wavelength of 477 nm. Its intensity was proportional to the amplitude of the effective excitation wavelength. Figure 3.7 shows the absorption spectrum simulated in Zemax.

3.1.5 Elliptical cylinder optical model

To collect weak fluorescence and improve the sensitivity of the device, the physical characteristics of the elliptical focal points are utilized. A beam of light emanating from one focal point of the ellipse will, after a single reflection, focus on the other focal point of the ellipse as shown in Figure 3.8. The cavity in which the light is collected is an ellipsoid with sizes shown in Figure 3.8 and Figure 3.9. The sample is placed in one focal point and the cavity concentrates the light emitted by it at the other focal point. The inner surface of the elliptical cavity is still considered to be aluminum.

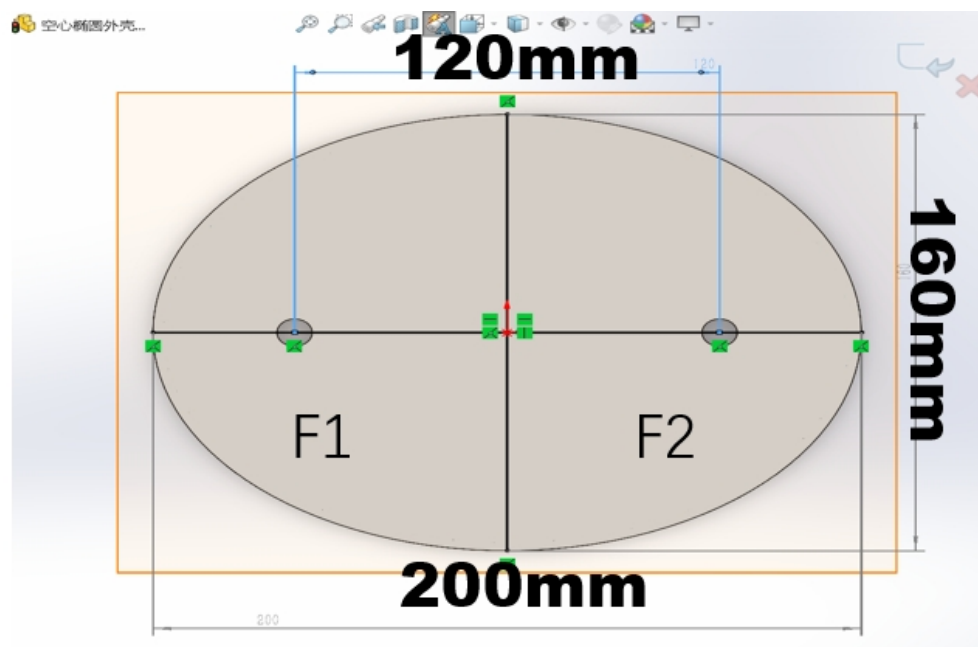


Figure 3.8: Elliptical cylinder reflective cavity: top view

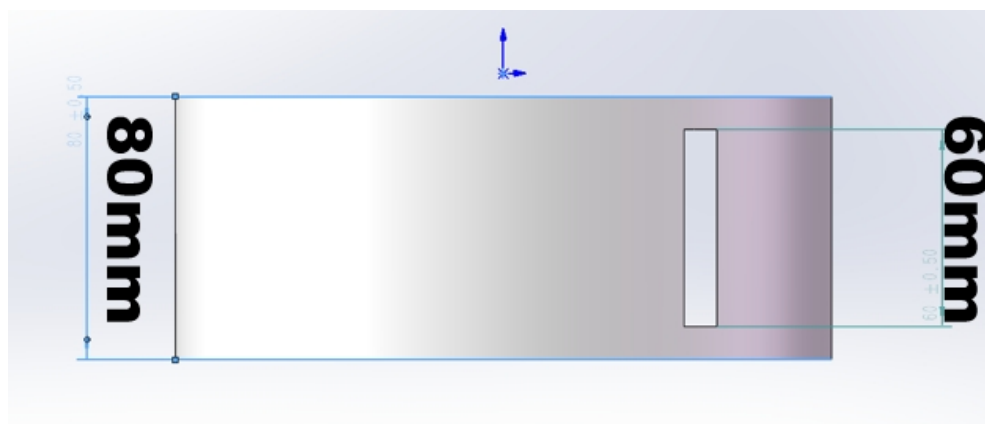


Figure 3.9: Elliptical cylinder reflective cavity: side view

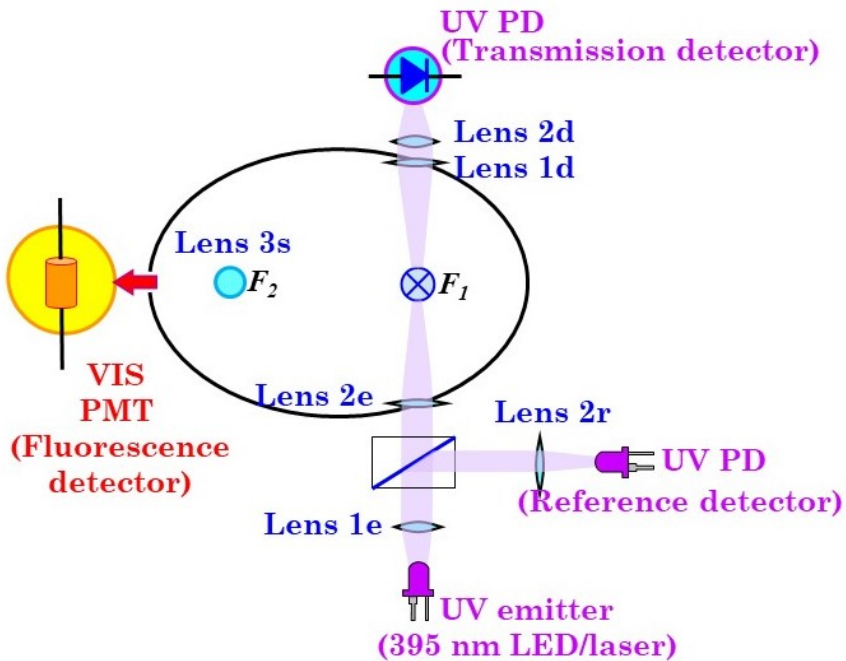


Figure 3.10: The full structure of the optical setup using the elliptical reflective cavity

The structure of the optical system design is shown in Figure 3.10 and its elements are detailed as follows.

1. **Excitation Light (LED):** An LED is used as the excitation light source although another convenient light source, e.g. a laser diode, may also be used. The light emitted by the LED then passes through a focusing lens to collimate its beam.
2. **Beam splitter:** It splits the excitation beam in 2 beams. One goes straight to the sample, the other is diverted to a reference photodetector, e.g. a photodiode (PD).
3. **Sample:** Located in the first focal point of the elliptical reflector, this is the target substance being analyzed. The excitation light, after passing through the filter, irradiates the sample, causing it to fluoresce.
4. **Cylindrical Lens + Cut-off filter:** The cylindrical lens located in the 2nd focal point of the elliptical cavity focuses most of the light sample, the light fluoresced by the sample and transmits it to the photodetector through a long-pass filter (not shown in Fig. 3.10) which blocks any excitation light.

5. **Photodetector (PMT):** It receives and detects the fluorescence signal transmitted from the sample, converting it into an electrical signal for analysis.

Figure 3.11 shows the results of our ZEMAX ray tracing simulations, where the black and yellow lines represent the structural lines of the CAD model in ZEMAX software, not light rays. The light emitted from one focal point is reflected by the elliptical cavity's outer wall and the upper and lower surfaces, and ultimately converges at the other focal point.

The fluorescent light emitted by fluorescein is isotropically emitted in all directions. Hence, in a traditional system, only a small part of the fluoresced light reaches the photodetector. The ZEMAX simulations results shown in Fig.3.11 confirm that the usage of the elliptical reflective cavity drastically increase the amount of collected fluorescent light and will thus significantly improve its detection efficiency.

In our ZEMAX simulations, the distribution of incoherent radiation intensity at the focal point was measured by using rectangular detector, and it can be seen that the light intensity converged in the cross-section at the focal point is the largest, which plays the role of concentrating light.

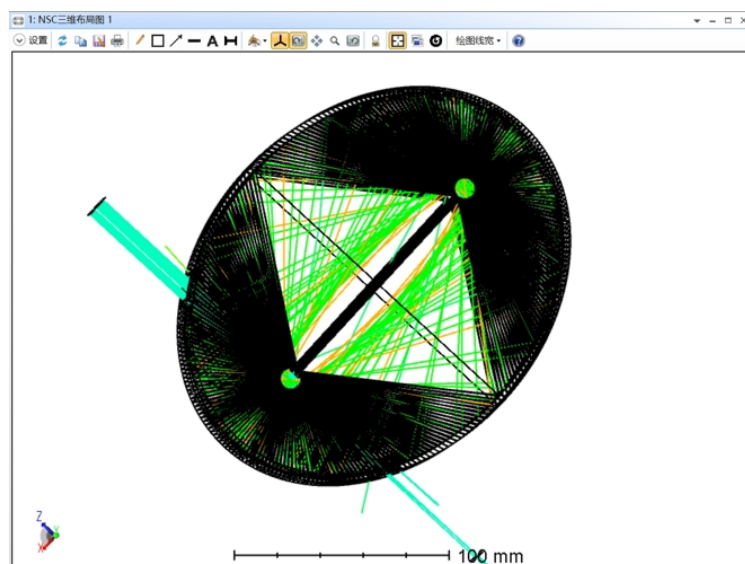


Figure 3.11: Results of our ZEMAX simulations inside the elliptical cavity: fluorescence light rays emitted from the first focal point converge at the second focal point.

3.1.6 Comparison of two reflective cavity models

Figures 3.12 and 3.13, compare ZEMAX simulations results obtained using the elliptical cylinder model and the integrating sphere model. The incoherent radiation intensity of the elliptical cylinder model is notably higher than that obtained in the integrating sphere model. This can be attributed to the lack of significant focusing effect in the integrating sphere model, resulting in a noticeably lower received power compared to the elliptical cylinder model. At this stage, using the same incident light source with a total emitted power of 2 W, simulating 100,000 rays for each model.

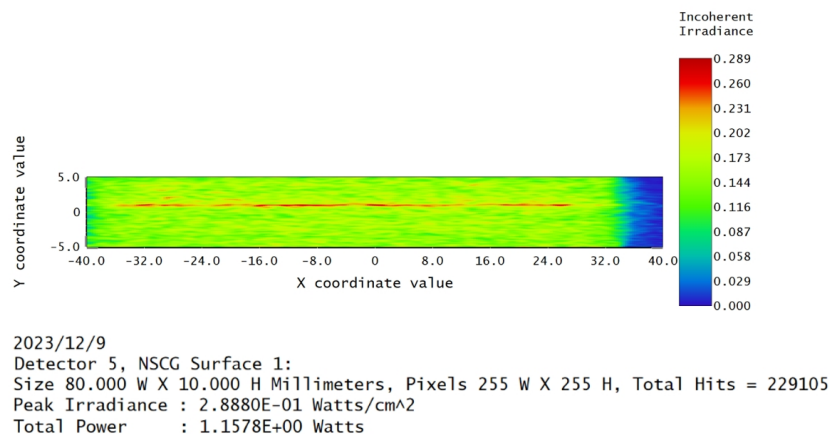


Figure 3.12: Light intensity arriving at the detector when using the elliptical

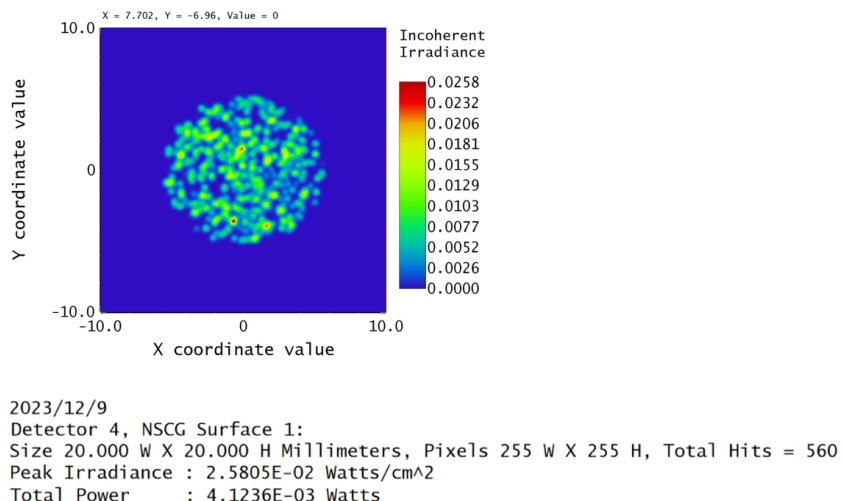


Figure 3.13: Light intensity arriving at the detector when using the integrating sphere model

Total Power Comparison

- **Elliptical Cylinder Model:**

- Peak irradiance: 288.8 mW/cm²
 - Total collected power: 1.1578 W

- **Integrating Sphere Model:**

- Peak Irradiance: 25.805 mW/cm²
 - Total collected power: 4.1236 mW

This comparison shows clearly that the total radiated power collected using the elliptical cylinder model is significantly higher than that of the integrating sphere model, indicating that the elliptical cylinder model is more efficient in collecting the emitted light.

We can now summarize the characteristic features of both models.

Integrating Sphere

Advantages

- **Non-Imaging:** There is no need for imaging in our application, thus reducing complexities in data interpretation and hardware requirements.
- **Comprehensive Light Collection:** Can collect light emitted in all directions, maximizing the captured fluorescence signal.

Challenges

- **Source Placement:** Fluorescence source must be inside the sphere, which can be restrictive and complicate the design.
- **Fabrication Difficulties:** Precise fabrication of spheres is challenging, leading to practical issues and increased costs.
- **Optimization Issues:** The design is not optimized for focusing all emitted fluorescence onto the detector, potentially reducing efficiency.

Elliptical cylinder

Advantages

- **Focusing Efficiency:** Placing the fluorescence source at one focal point (F1) and the detector at the other focal point (F2) utilizes the reflective properties of ellipses, enhancing focusing efficiency as theoretically the entire emitted fluorescence reaches the detector.
- **Improved Signal Collection:** The elliptical design can improve the collection of fluoresced light, ensuring higher sensitivity and better SNR.

Challenges

- **Reduced efficiency:** There is no real photodetector which can capture light from all around it (360 degree incidence). In practice, it is better to place a lens in the second focal point and transmit the light outwards, through a slit in the cavity wall to the photodetector (see again Fig.3.10). However, this means that not all the light focused onto the second focal point will reach the photodetector.
- **Complex implementation:** It requires careful fabrication to accurately realize the ideal elliptical shape and requires usage of a highly reflective material.

Conclusion

The transition from an integrating sphere to an ellipse model marks an evolution towards improving fluorescence collection efficiency. The integrating sphere faces significant challenges in source placement and fabrication. In contrast, the elliptical cavity model offers superior focusing of emitted fluorescence onto the detector, enhancing overall efficiency and effectiveness, even when not all the light (incoming to the second focal point) can be directed onto the photodetector. Therefore, we have chosen the elliptical reflector given its easier implementation and superior performance.

Chapter 4

Circuit design

4.1 Hardware Circuit Overall Design

A complete photoelectric signal detection and processing system mainly consists of light signal acquisition, photoelectric conversion, weak electrical signal amplification, MCS51 microcontroller control, and signal display and processing on the host computer. The overall system scheme is shown in Figure 4.1.

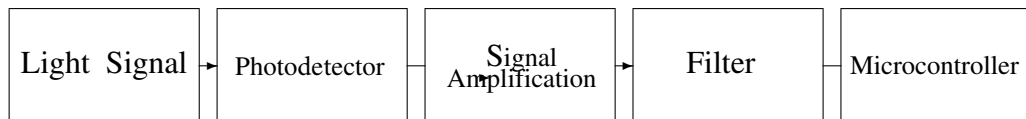


Figure 4.1: System Overall Scheme Diagram

The system uses a photodiode as the photoelectric conversion device, converting weak light signals into weak electrical signals. Since the output current of the photodiode is very small and easily affected by noise, the design uses the TLC2262 integrated chip from Texas Instruments, which has excellent low-noise pre-amplification characteristics, to amplify the weak electrical signals, thus driving the subsequent circuit. To achieve sufficient amplification of the weak signals, a two-stage amplification design is adopted, with the second stage using the TL064. After amplification, the signal still contains noise, so the design includes filtering to process the signal. The amplified and filtered signal is sent to the

C8051F040 microcontroller, which has strong processing power and built-in ADC circuits, to control the entire signal acquisition.

4.2 Hardware Design

4.2.1 Design of the Photoelectric Conversion Circuit

The primary requirement for weak photoelectric signal detection and acquisition is to convert weak light signals into electrical signals. Therefore, the photoelectric conversion capability of the circuit is crucial for the performance of the weak photoelectric detection and acquisition system. Several common photoelectric detection devices were introduced in Chapter 2. In practical applications, to convert photoelectric signals without distortion, the photoelectric detection device should match the light signal being measured and the subsequent circuit in terms of operating characteristics and parameters. This ensures that each component of the system operates under optimal conditions, achieving the best system performance. The key points for selecting photoelectric detection devices are summarized as follows:

- The photoelectric detection device should match the spectral characteristics of the light source. Different types of detectors should be used for different wavelengths, such as UV photodetectors for Ex light, and silicon photodetectors for visible light.
- The alignment of the device with the position of the concentrated incident radiation energy is crucial. Typically, the variation center of the incident radiation flux should be within the linear region of the photoelectric de-tention device to achieve good linear detection.
- High sensitivity is essential for detecting weak photoelectric signals to out-put sufficiently strong electrical signals.
- Different photoelectric detection devices should be chosen based on the frequency and modulation mode of the light signal being detected. The response time and upper frequency limit of the device are

important criteria, and electrical characteristics matching with the subsequent circuit is also critical.

In our optoelectronic conversion circuit, the photodetector used is a photodiode, selected based on the actual characteristics of the circuit. A PIN diode is a type of photodiode. Essentially, it is a converter that transforms optical variations into current and then into voltage. As shown in Figure 4-2, the structure mainly places the intrinsic (undoped) semiconductor between the P-type and N-type semiconductors, increasing the distance of the PN junction and thus reducing the junction capacitance. This type of photodiode has a relatively wide bandwidth, reaching up to 10 GHz; however, its drawback is the relatively small output current, which can only reach a few microamperes to tens of microamperes.

Sensitivity of Photodiodes

The current sensitivity of a photodiode (e.g. a PIN diode like the one shown in Fig.4.2) is defined as the ratio of the change in photocurrent to the change in irradiance on the photosensitive surface. That is,

$$S_i = \frac{dI}{d\Phi} = \frac{\eta q \lambda}{hc} (1 - e^{-\alpha d}) \quad (4.1)$$

where Φ is the incident light flux, I is the photogenerated current intensity, η is the photodetector's quantum efficiency, α is the absorption coefficient in the photodetector's material (wavelength-dependent) and d is the distance along which the light propagates and is absorbed in the photodetector.

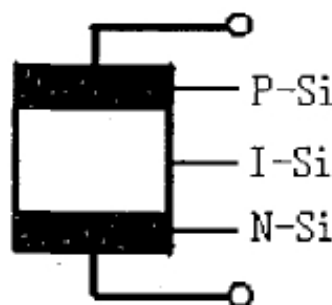


Figure 4.2: PIN photodiode structure

Spectral Response Curve

When monochromatic light of different wavelengths is incident on the photodiode at the same power level, the relationship between current sensitivity and wavelength is the spectral response of the photodiode. Generally, the spectral response curves of photodiodes made of different materials are different. Figure 4.3 shows the spectral response curves of photodiodes made of four typical materials. As shown in the figure, the spectral response range of GaAs material is the widest, while Ge material has the narrowest spectral response range. The spectral response range of Si material lies between these two, with a long wavelength limit of about $1.1\text{ }\mu\text{m}$ and a short wavelength limit of about $0.4\text{ }\mu\text{m}$, with the peak response wavelength being approximately $0.9\text{ }\mu\text{m}$.

Response Time

When frequency-modulated optical radiation acts on the PN junction of a silicon photodiode, the photodiode current undergoes the following process:

- (1) The time taken for photogenerated carriers to drift across the depletion region in the PN junction, denoted as τ_d .

If the drift velocity of the carriers in the depletion region is v_d and the width of the depletion region is W , the maximum drift time within the junction is:

$$\tau_d = \frac{W}{v_d} \quad (4.2)$$

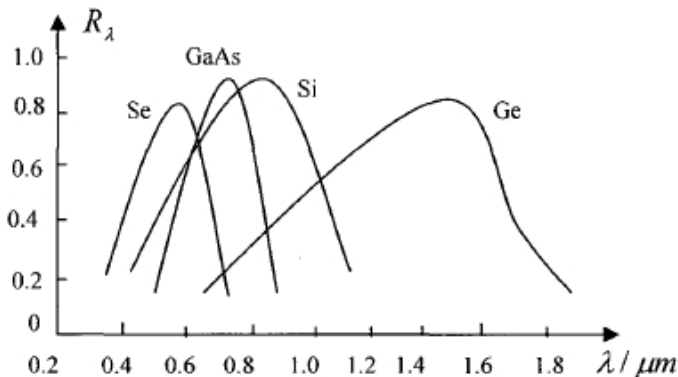


Figure 4.3: Spectral response curves of photodiodes made of common semiconductors

Under normal circumstances, the electric field strength E inside the depleted region of a photodiode is greater than 10^5 V/cm , the width of the depletion region W is approx. $100 \mu\text{m}$, and the average drift velocity of the carriers is higher than 10^7 cm/s . Hence, using equation (4.2), the drift time τ_d results of about 1 ns.

(2) Due to the capacitance C_j within the PN junction, the intrinsic resistance R of the photodiode, and the load resistance R_L forming the RC network, the RC delay time τ_{RC} is:

$$\tau_{RC} = (R + R_L)C_j \quad (4.3)$$

For a typical photodiode, the capacitance C_j of the PN junction is generally several pF, and the intrinsic resistance R is about 250Ω . According to equation (4-3), when the load resistance R_L is $< 0 \Omega$, the calculated delay time τ_{RC} is also in the nsrange. However, the delay time will increase when the load resistance increases.

(3) The time required for photogenerated carriers generated outside the PN junction to diffuse into the PN junction, denoted as τ_p .

Since for a general PN junction photodiode, photogenerated carriers generated outside the depletion region by incident radiation must diffuse to the boundary of the built-in electric field within the junction and then be drifted to the P and N regions, the diffusion of carriers is usually slow, so the diffusion time τ_p is relatively long, about 100 ns. Therefore, combining the above three factors affecting the response time, the main factor limiting the response time of the PN junction photodiode is the diffusion time τ_p .

There are two main types of optical detection modes widely used in photodiodes. One is called the photovoltaic mode. This mode requires applying a reverse bias voltage across the photodiode, which will generate dark current and nonlinearity. This mode can be used for high-speed applications; the photodiode is merely a passive component. The other is the photo-conductive mode, where the photodiode is under zero bias, with no power supply required. The current flows, and the linearity is better, making this mode suitable for precision measurement systems. This dissertation mainly discusses

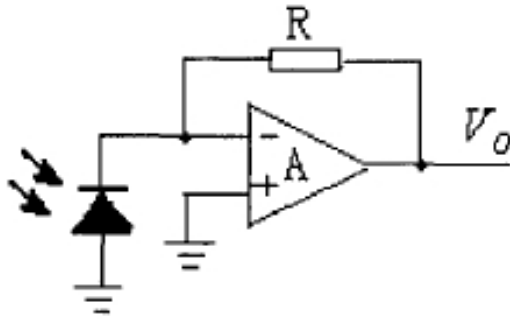


Figure 4.4: Typical photodetection circuit (transimpedance amplifier).

the photovoltaic mode. A typical optical detection circuit is shown in Figure 4.4.

In practical applications, various noises in the circuit must be considered. The primary noise sources are the thermal noise of the components and the noise of the load resistance R_L . The average voltage value of the thermal noise U_T is determined by the temperature of the material, given by the following equation:

$$U_T^2 = 4kTR \int_0^{f_1} R(f)df \quad (4.4)$$

In equation (4.4), k is Boltzmann's constant, T is the absolute temperature in Kelvin, and the change in resistance value with frequency is denoted as $R(f)$.

The bandwidth of the thermal noise (in Hertz) is:

$$\Delta f = \frac{kT}{h} \eta^2 / 6 \quad (4.5)$$

where h is Planck's constant, and η is a dimensionless efficiency factor.

Assuming a typical room temperature of 300 K and $\eta \approx 1$, we obtain:

$$\Delta f \approx \frac{(1.38 \times 10^{-23} \times 300)}{6.626 \times 10^{-34}} \frac{1}{6} \approx 10.28 \text{GHz}$$

In practical weak optical signal detection, the noise voltage is determined by the bandwidth $\Delta f = f_2 - f_1$ of the signal collection and processing circuit. Therefore, equation (4.4) can be simplified as:

$$U_T^2 = 4kTR\Delta f \quad (4.6)$$

The corresponding average value of the thermal noise current is:

$$I_T^2 = \frac{U_T^2}{R^2} = \frac{4kTR\Delta f}{R^2} = \frac{4kT\Delta f}{R} \quad (4.7)$$

According to equation (4.7), the thermal noise voltage and current can be obtained in a typical situation ($T=300K$):

$$U_T = \sqrt{4kTR\Delta f} = 1.29 \times 10^{-10} \sqrt{R\Delta f} \quad (4.8)$$

$$I_T = \sqrt{\frac{4kT\Delta f}{R}} = 1.29 \times 10^{-10} \sqrt{\frac{\Delta f}{R}} \quad (4.9)$$

When the resistance $R = 1 k\Omega$ and assuming the bandwidth $\Delta f = 200MHz$, the thermal noise voltage is:

$$U_T = 1.29 \times 10^{-10} \sqrt{10^3 \times 2 \times 10^8} = 57.7 \mu V \quad (4.10)$$

And the corresponding thermal noise current is:

$$I_T = 1.29 \times 10^{-10} \sqrt{\frac{2 \times 10^8}{10^3}} = 1.3 nA \quad (4.11)$$

Equation (4.11) shows that in the signal detection and processing circuit, when the resistance R constant, the thermal noise voltage is directly proportional to the square root of the bandwidth Δf , and the noise current is inversely proportional to the square root of the resistance.

Therefore, based on basic circuit knowledge, a feedback resistor R and a parallel capacitor C_1 are added to the operational amplifier to reduce low-frequency noise. The improved optoelectronic conversion circuit is shown in Figure 4.5.

Based on the introduction in Chapter 2, the average value of the shot noise current I_s^2 can be expressed as:

$$I_s^2 = 2qI_p\Delta f \quad (4.12)$$

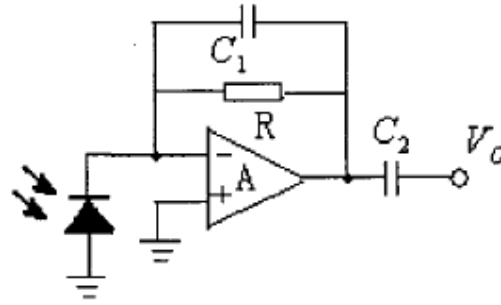


Figure 4.5: Improved transimpedance amplifier

In equation (4.12), I_p represents the average value of the photocurrent, and q represents the electron charge. Thus, the noise current value represented by I_s and the noise voltage U_s generated at both ends of the load can be respectively expressed as:

$$I_s = \sqrt{2qI_p\Delta f} \quad (4.13)$$

$$U_s = I_s R = R \sqrt{2qI_p\Delta f} \quad (4.14)$$

The photocurrent generated by the PIN diode selected for this system is of approximately $5.6 \mu A$, so the shot noise voltage is:

$$U_s = R \sqrt{2qI_p\Delta f} = 18.9 \mu V \quad (4.15)$$

Then, the total noise output current is:

$$I_N = \sqrt{I_T^2 + I_s^2} = \left(\frac{1}{R}\right) \sqrt{U_T^2 + U_s^2} = 60.7 \times 10^{-3} \mu A \quad (4.16)$$

The total noise voltage is:

$$V_N = I_N R = 60.7 \times 10^{-3} mV \quad (4.17)$$

Therefore, the signal-to-noise ratio (SNR) of the optoelectronic conversion is:

$$SNR = \frac{I_p}{I_N} = \frac{5.6}{60.7 \times 10^{-3}} = 92.2 \quad (4.18)$$

In summary, the improved optoelectronic conversion circuit has the characteristics of low noise voltage and high signal-to-noise ratio, meeting the design requirements.

4.3 Design of the Preamplifier Circuit

Photodiodes receive the optical signal and convert it into a weak current signal, usually in the μA range. The photodiode's signal is converted into a voltage signal through the feedback resistor and operational amplifier configuration, and only after passing through the amplification and processing stages can the signal be recorded. The California Institute of Technology has conducted in-depth experimental research on the detection of weak optical signals using photodiodes and various types of amplifiers, providing extensive data. This research demonstrates the importance of using high-performance preamplifiers in weak optical signal detection systems.

4.3.1 General Amplification Circuit

The basic amplification circuit is shown in Figure 4.6. For an ideal operational amplifier, the feedback input terminals satisfy the characteristics of "virtual short" and "virtual open". We can obtain:

$$V_O = -\frac{R_f}{R_1} V_i \quad (4.19)$$

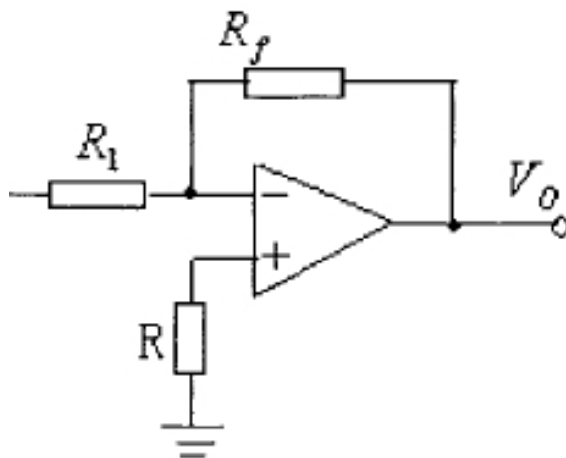


Figure 4.6: Transimpedance amplifier

V_O and V_i have a linear proportional relationship, so if the voltage amplification factor needs to be changed, it can be achieved by changing R_f . However, in practical circuit applications, operational amplifiers cannot achieve the ideal state, which affects the linear conversion accuracy of the circuit, leading to conversion errors. At the same time, the feedback resistor R_f also affects the sensitivity of the photodetection. To improve sensitivity, R_f must be increased, but this requires the resistor to have excellent insulation properties. These factors can reduce system stability. Moreover, increasing R_f will also increase the thermal noise current of the resistor, which should be avoided in practical applications.

4.3.2 T Network Amplification Circuit

The T network amplification circuit is also commonly used in circuits and can be used in photodetection circuits. Its structure is shown in Figure 4.7. From the figure, based on circuit theory, assuming ideal conditions, the relationship between the output voltage V_O and the input voltage V_i can be obtained as:

$$V_O = -\frac{R_S}{R_1} \left(1 + \frac{R_X}{R_S} + \frac{R_X}{R_2} \right) V_i \quad (4.20)$$

Thus, the gain A_V of the amplification circuit under ideal conditions can be derived as:

$$A_V = \frac{V_O}{V_i} = -\frac{R_S}{R_1} \left(1 + \frac{R_X}{R_S} + \frac{R_X}{R_2} \right) \quad (4.21)$$

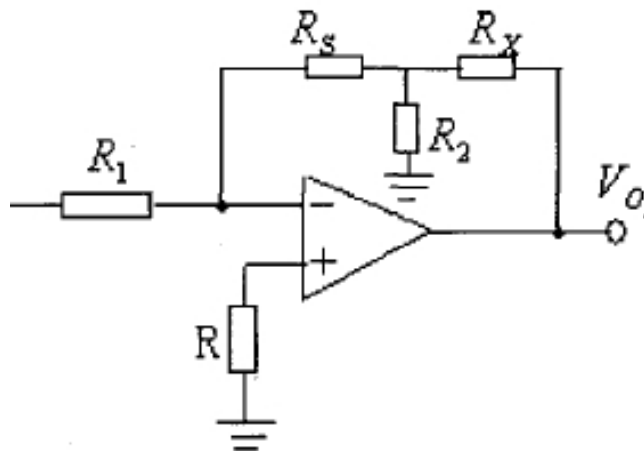


Figure 4.7: T Network Amplification Circuit

When $R_X \cdot R_2 \ll R_S$, and the open-loop gain $A \gg 1$, we have:

$$V_O = -\frac{R_S}{R_1} \left(1 + \frac{R_X}{R_2} \right) V_i \quad (4.22)$$

Therefore, the different resistance values in the network directly determine the gain of the amplifier. This resistive structure makes the amplifier more precise and stable. At the same time, due to the feedback resistance extending by a factor of $\left(1 + \frac{R_X}{R_2}\right)$, it can reduce the influence of thermal noise and minimize the impact of bias current on the input of the amplifier. However, it should be noted that when there is a single-ended input, if the input is an unstable differential signal, the unstable differential signal will directly affect the output stability of the circuit, thus reducing the circuit's stability.

Differential Preamplifier Circuit

The differential amplifier circuit has strong suppression capability for common-mode signals. It is very effective in reducing the dark current of components and the influence of ambient temperature changes on the circuit in photodetection systems. The differential amplifier circuit is shown in Figure 4.8.

In the circuit, the main function of the bypass capacitor C is to prevent oscillation and reduce the ripple in the output DC level. From the circuit, we can see that the relationship between the output V_O of the differential amplifier circuit and the inverse input terminals V_1 and V_2 is:

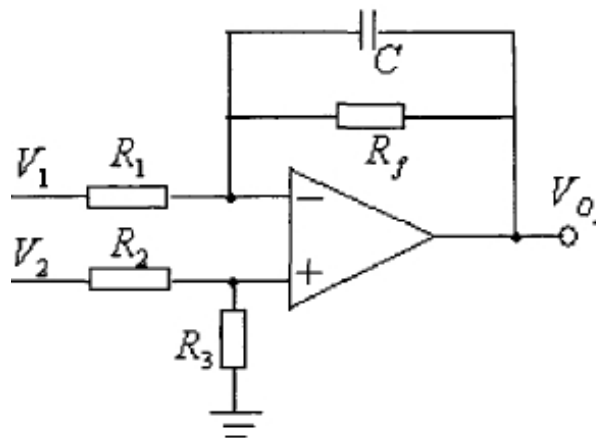


Figure 4.8: Differential Amplifier Circuit

$$V_O = -\frac{R_f}{R_1}V_1 + \left(\frac{R_3}{R_2+R_3}\right) \left(1 + \frac{R_f}{R_1}\right) V_2 \quad (4.23)$$

When $R_1 = R_2$ and $R_3 = R_f$, we have:

$$V_O = -\frac{R_f}{R_1}V_1 + \frac{R_f}{R_1}V_2 = \frac{R_f}{R_1}(V_2 - V_1) \quad (4.24)$$

However, this differential amplifier circuit has high requirements for impedance matching. If the resistors are not matched, significant dynamic errors can be introduced into the circuit.

4.3.3 Instrumentation Amplifiers

In the field of electronic technology, instrumentation amplifiers are a type of amplifier with differential inputs and single-ended outputs. Their basic operation is similar to differential amplifiers, but they have better performance. For traditional differential amplifiers, the main issue is the precise matching of resistors, while instrumentation amplifiers can complete the difference signal amplification under better conditions and have strong common-mode rejection capabilities. This is very useful in weak optical signal detection circuits.

The key performance characteristics of instrumentation amplifiers are:

- 1) High common-mode rejection ratio (CMRR)

In instrumentation amplifiers, the ratio of differential gain A_d to common-mode gain A_c is defined as the common-mode rejection ratio (K_{CMR}):

$$K_{CMR} = 20 \log \left(\frac{A_d}{A_c} \right) \quad (4.25)$$

- 2) High input impedance

The high input impedance is very beneficial for detecting weak signals. Because general sensors have high output impedance, it is required that the subsequent circuits of the optical sensor must have high input impedance.

3) Symmetrical output mode

The circuit's symmetrical output can eliminate common-mode noise in the system to a certain extent. Therefore, using this type of amplifier can meet the requirements of sensors for amplification circuits.

4) Adjustable offset voltage and bias current

The internal components of instrumentation amplifiers are usually manufactured on the same chip, so they are relatively unaffected by temperature variations, have high accuracy, and have low noise. Moreover, they can reduce the offset voltage and bias current drift of the amplifier circuits.

5) Various connection modes

Different connection modes can be selected according to different requirements. Generally, the connection mode should be chosen to minimize the common-mode signal while maintaining good symmetry.

In this design, we selected the TLC2262 chip from Texas Instruments [40], which has a high CMRR, low noise, and low offset voltage. According to equations (4.11) and (4.12), the output voltage of the optical sensor under weak optical signals can reach the microvolt level, requiring an amplification factor of 10^3 to 10^6 . The initial amplification was set to 10^3 , and the subsequent amplification can be achieved through additional stages. The use of instrumentation amplifiers ensures that the amplified signal can be effectively processed with minimal distortion, achieving the desired signal-to-noise ratio. The final output signal meets the design requirements with an amplification factor of 500.

The instrumentation amplifier is ideal for accurate amplification of weak differential signals. The choice of component values (resistors and operational amplifiers) is primarily to ensure the precision, stability, and specific gain of the circuit. The explanations for the selection of the component values used in our circuit shown in Fig.4.9 are as follows:

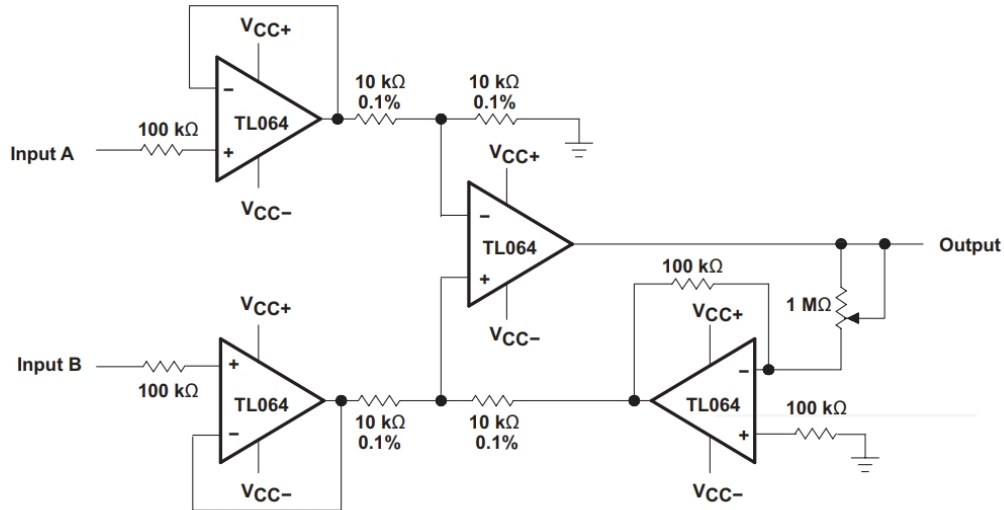


Figure 4.9: Instrumentation amplifier [39].

The resistors ($100\text{ k}\Omega$) used at each input terminal are mainly to match the input impedance, reduce the impact of input bias current on the circuit, and provide some current protection.

The gain-setting resistors ($10\text{ k}\Omega$, 0.1%) are used to set the gain of the circuit. Using resistors with $0.1\% 0.1\%$ tolerance is necessary in order to ensure the accuracy and consistency of the gain. The resistor network formed by two $10\text{ k}\Omega$ resistors ensures a high common-mode rejection ratio (CMRR) of the amplifier, effectively suppressing common-mode noise.

The feedback resistor ($1\text{ M}\Omega$) is used to set the gain of the differential amplifier. The formula for the gain is:

$$G = 1 + \frac{2R_2}{R_1} \quad (4.26)$$

where R_1 is $10\text{ k}\Omega$ and R_2 is $1\text{ M}\Omega$. Therefore, the gain of the circuit is:

$$G = 1 + \frac{2 \times 1,000,000}{10,000} = 201$$

The choice of $1\text{ M}\Omega$ is to achieve the required high gain.

TL064 comprises low-power, high-input impedance operational amplifiers, which are very suitable for precise instrumentation amplifier circuits.

Their low offset voltage and low noise characteristics allow them to accurately amplify weak signals.

The selection of these component values is to achieve the required amplification factor while ensuring high precision and effectively suppressing noise and other interferences.

4.3.4 Design of the Control Unit Circuit

The system's acquisition and control part is composed of the C8051F040 microcontroller. The C8051F040 is fully compatible with the 8051 and 8031 instruction sets and is a fully integrated mixed-signal system-level MCU chip with 64 digital I/O pins. It is suitable for application systems that require strong hardware functionality, fast computing speed, harsh working environments, high reliability, strong expansion capabilities, and low power consumption. Its main features are as follows:

- Controller Area Network (CAN) controller with 32 message objects, each with its own identifier.
- A 10-bit ADC with 8 channels and an analog multiplexer.
- Two 16-bit programmable counter arrays with capture/compare modules.
- Byte-programmable Flash memory with 16K bytes of on-chip data memory.
- 256 bytes of internal data memory.
- Addressable 64K bytes of external data memory space.
- Operating voltage range from 2.7V to 5.5V.
- Hardware-implemented SPI, UART, and two I2C serial interfaces.
- Two general-purpose 16-bit timers.
- On-chip watchdog timer, power monitor, and temperature sensor.

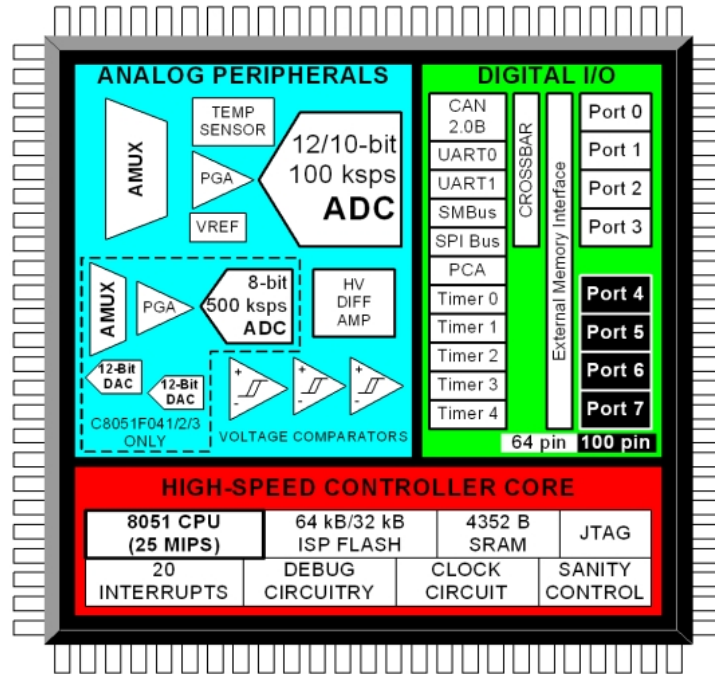


Figure 4.10: Microcontroller structure block diagram

The block diagram of its structure is shown in Figure 4.11.

This circuit diagram is a typical wiring diagram for a microcontroller system. Below is the analysis and explanation of the functions of each part: The microcontroller is a CS91F840 model with 100 pins connected to various external components. The power supply section: The VDD pins (9, 16, 50, 69, 98) provide the working voltage for the microcontroller. There are two $10\mu F$ capacitors and two 104 ($0.1\mu F$) capacitors used for power filtering to remove power supply noise. The VSS pins (6, 12, 14, 22, 50, 88) are ground pins used to provide a reference ground for the circuit. The oscillator section: The X1 and X2 pins (26, 27) are connected to an external crystal oscillator and two $33pF$ capacitors to provide the clock signal for the microcontroller.

The input section: Two buttons are connected to the P0.1 and P0.2 pins, with pull-down resistors to ground, used for user input. The LED section: Multiple LEDs are connected to the P1.0 to P1.7 and P2.0 to P2.7 pins with current-limiting resistors to ground for indicator display. The analog sec-

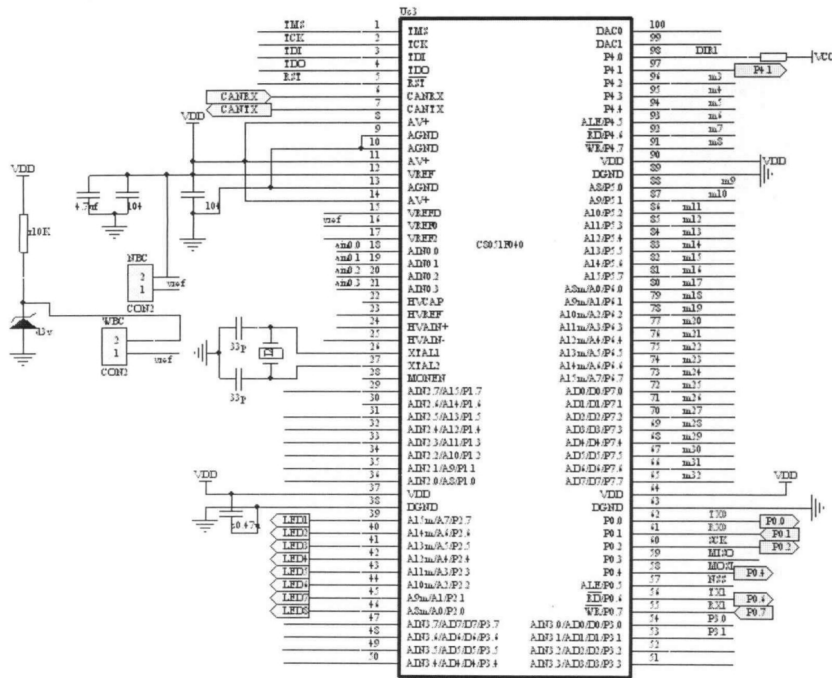


Figure 4.11: Microcontroller circuit

tion: Multiple ADC pins (ADC0 to ADC3 pins 19, 20, 21, 22) are used for analog signal acquisition. The communication interface: The JTAG interface (TMS, TCK, TDI, TDO pins 1, 2, 3, 4) is used for microcontroller programming and debugging. The CAN interface (CANRX, CANTX pins 7, 8) is used for Controller Area Network (CAN) communication. The function pins: Various general-purpose input/output (GPIO) pins are used for connecting external devices and sensors. The reset pin (RST pin 5) is connected to the reset circuit. The interface circuit: Used for connecting external sensors and modules through GPIO and ADC pins. In summary, this circuit diagram shows a complex microcontroller system that stabilizes the power supply with multiple filtering capacitors, uses an external crystal oscillator to provide the clock signal, is programmed and debugged via the JTAG interface, connects to LED displays and button inputs, includes multiple ADC pins for analog signal acquisition, and communicates through the CAN interface. This circuit is well-suited for embedded system development and debugging, making it a typical microcontroller application circuit.

4.4 Summary of this Chapter

This chapter introduced the specific hardware circuit design for weak light signal detection and acquisition. The design principles of the main hardware units, including the light signal detection circuit, preamplifier circuit were provided along with circuit diagrams and analysis calculations.

Chapter 5

Conclusion and Future Work

5.1 Conclusion

This thesis successfully developed an optical detection system capable of efficiently detecting low-intensity light signals. By employing an elliptical cylinder optical model, the system achieved higher light collection efficiency compared to traditional integrating sphere models. The hardware design, including the photoelectric conversion circuit and amplification stages, demonstrated the capability to amplify weak signals with minimal noise, meeting the stringent requirements for sensitive optical detection.

The use of advanced materials and precise alignment techniques in the optical model significantly improved the system's overall performance. The incorporation of a C8051F040 microcontroller facilitated robust control and data acquisition, ensuring reliable operation even in harsh environmental conditions. The project's findings highlight the potential of the developed system for practical applications in water purity analysis and other fields requiring sensitive light detection.

5.2 Future work

Future work will focus on optimizing the optical alignment process to ensure maximum efficiency in light collection and signal amplification, exploring automated alignment techniques and advanced calibration methods. Additionally, integrating sophisticated signal processing algorithms, such as machine learning techniques, will enhance detection accuracy and reliability by better distinguishing between signal and noise. Efforts will also be made towards miniaturizing and making the detection system more portable, facilitating field deployment and on-site analysis by integrating miniaturized components and optimizing power consumption.

References

- [1] Singapore Public Utilities Board. *Singapore's Water Story: Sustainability and Innovation*. PUB Singapore, 2015.
- [2] H. Michaels and J. Smith. Development of low intensity light detection for optical analysis. *Journal of Environmental Sciences*, 35:45–60, 2020.
- [3] J. R. Lakowicz. *Principles of Fluorescence Spectroscopy*. Springer, 2006.
- [4] B. Valeur. *Molecular Fluorescence: Principles and Applications*. Wiley-VCH, 2002.
- [5] G. G. Guilbault. *Practical Fluorescence: Theory, Methods, and Techniques*. Marcel Dekker, 1990.
- [6] F. Hammes and T. Egli. Fluorescence-based analytical methods for microbial cells. *Applied and Environmental Microbiology*, 71:759–768, 2005.
- [7] J. Sambrook and D. W. Russell. *Molecular Cloning: A Laboratory Manual*. Cold Spring Harbor Laboratory Press, 2001.
- [8] H.-H. Perkampus. *UV-VIS Spectroscopy and Its Applications*. Springer, 1992.
- [9] J. R. Albani. *Principles and Applications of Fluorescence Spectroscopy*. Wiley, 2007.
- [10] O. S. Wolfbeis. Fluorescence methods and applications: Spectroscopy, imaging, and probes. *Chemical Reviews*, 111:2361–2415, 2011.
- [11] J. N. Demas. *Excited State Lifetime Measurements*. Academic Press, 1983.

- [12] BMG LABTECH. Fluorescence intensity, 2024. Accessed: 2024-07-12.
- [13] Joseph R Lakowicz. *Principles of Fluorescence Spectroscopy*. Springer Science & Business Media, 2006.
- [14] Bernard Valeur and Mario N Berberan-Santos. *Molecular Fluorescence: Principles and Applications*. John Wiley & Sons, 2012.
- [15] Laurence M Loew. *Spectroscopic Membrane Probes*. CRC Press, 2010.
- [16] Otto S Wolfbeis. *Fluorescence: Basics, Methods and Applications*. Springer, 2015.
- [17] Robert F Chen. Fluorescence quantum yields of tryptophan and tyrosine. *Analytical Biochemistry*, 21(2):339–342, 1967.
- [18] Ralph Weissleder and Vasilis Ntziachristos. Shedding light onto live molecular targets. *Nature Medicine*, 9(1):123–128, 2003.
- [19] Scott Kable. Basic principles of fluorescence. In *Fundamentals of Fluorescence Imaging*, pages 1–34. Jenny Stanford Publishing, 2019.
- [20] J. R. Albani. *Principles and Applications of Fluorescence Spectroscopy*. Wiley-Blackwell, 2007.
- [21] . . . , 2009.
- [22] Shi-Wei Lin, Chih-Han Chang, and Che-Hsin Lin. High-throughput fluorescence detections in microfluidic systems. *Journal of Microfluidic Systems*, 15(3):123–135, 2020.
- [23] Bingcheng Yang, Feng Tan, and Yafeng Guan. A collinear light-emitting diode-induced fluorescence detector for capillary electrophoresis. *Talanta*, 65:1303–1306, 2005.
- [24] Bingcheng Yang, Feng Tan, and Yafeng Guan. A collinear light-emitting diode-induced fluorescence detector for capillary electrophoresis. *Talanta*, 65:1303–1306, 2005.

- [25] Chongde Zi, Junsheng Shi, Yonghang Tai, Huan Yang, and Xicai Li. Design of portable time-resolved fluorometer. *Advances in Bioscience and Bioengineering*, 4(6):79–84, 2016.
- [26] Alan V. Oppenheim and Ronald W. Schafer. *Digital Signal Processing*. Prentice-Hall, 1975.
- [27] Graham Smith and B.T. Dent. *Scientific Measurement and Analysis*. Oxford University Press, 1997.
- [28] M. L. Meade. *Lock-in Amplifiers: Principles and Applications*. Peter Peregrinus Ltd., 1983.
- [29] Jerry C. Whitaker. *AC Power Systems Handbook*. CRC Press, 2002.
- [30] Steven M. Kay. *Modern Spectral Estimation: Theory and Application*. Prentice-Hall, 1988.
- [31] Simon Haykin. *Adaptive Filter Theory*. Prentice Hall, 1991.
- [32] Harry L. Van Trees. *Detection, Estimation, and Modulation Theory*. Wiley, 2001.
- [33] Steven M. Kay. *Fundamentals of Statistical Signal Processing: Detection Theory*. Prentice Hall, 1998.
- [34] Athanasios Papoulis and S. Unnikrishna Pillai. *Probability, Random Variables, and Stochastic Processes*. McGraw-Hill, 2002.
- [35] Zurich Instruments. *Introduction to Lock-in Amplifiers*. Zurich Instruments, 2020. Accessed: 2024-07-04.
- [36] Steven W. Smith. *Digital Signal Processing: A Practical Guide for Engineers and Scientists*. Newnes, 2019.
- [37] Alan V. Oppenheim, Alan S. Willsky, and S. Hamid Nawab. *Signals and Systems*. Prentice Hall, 2020.

- [38] Simon Haykin. *Adaptive Filter Theory*. Pearson, 2018.
- [39] Glenn F. Knoll. *Radiation Detection and Measurement*. Wiley, 2018.
- [40] Texas Instruments. *TLC2262 Operational Amplifier Data Sheet*, 2023. Accessed: 2024-07-14.